Article

Quantitative Proteomic Characterization of Foreign Body Response towards Silicone Breast Implants Identifies Chronological Disease-Relevant Biomarker Dynamics

Ines Schoberleitner [1], Klaus Faserl [2], Bettina Sarg[2], Daniel Egle [3], Christine Brunner [3] and Dolores Wolfram [1,*]

[1] Department of Plastic, Reconstructive and Aesthetic Surgery; Medical University of Innsbruck, Anichstraße 35, A-6020 Innsbruck
[2] Protein Core Facility, Institute of Medical Chemistry, Biocenter, Medical University of Innsbruck, Innrain 80-82, A-6020 Innsbruck
[3] Department of Obstetrics and Gynecology; Medical University of Innsbruck, Anichstraße 35, A-6020 Innsbruck
* Correspondence: dolores.wolfram@i-med.ac.at; Tel.: +43 512 504 82050

Abstract: The etiology of exaggerated fibrous capsule formation around silicone mammary implants (SMI) is multifactorial but primarily induced by immune mechanisms toward the foreign material silicone. The aim of this work was to enlighten the disease progression from implant insertion and immediate tissue damage response reflected in (a) the acute wound proteome, and (b) the adsorption of chronic inflammatory wound proteins at implant surfaces. An intra-individual absolute quantitation TMT-liquid chromatography-tandem mass spectrometry approach was applied to profile wound proteome formed around SMI the first five days post-implantation. Compared to plasma, the acute wound profile resembled a more complex composition comprising plasma-derived and locally differentially expressed proteins (DEPs). DEPs were subjected to functional enrichment analysis, which revealed the dysregulation of signaling pathways mainly involved in immediate inflammation response and ECM turnover. Moreover, we **found** time-course variations in protein enrichment immediately post-implantation and adsorbed to SMI surfaces after 6-8 months. Characterization of the expander-adhesive proteome by label-free approach **uncovered** a long-term adsorbed acute wound and the fibrosis-associated proteome. Our findings propose a wound biomarker panel for the early detection and diagnosis of excessive fibrosis that could potentially broaden insights into the characteristics of fibrotic implant encapsulation.

Keywords: SMI (silicone mammary implants); FBR (foreign body response); wound healing; wound infection; capsular fibrosis; implant encapsulation; early-stage fibrosis; surface adsorption; immunomics; biomarkers

1. Introduction

Fibrosis is a hallmark of numerous pathological conditions, marked by excessive production and accumulation of collagenous and non-collagenous extracellular matrix (ECM) components, leading to a loss of tissue architecture and organ function [1]. Initiated by some sort of injury and consecutive inflammation (e.g., persistent infections, autoimmune reactions, allergic responses, chemical insults, radiation, and tissue injury), the subsequent continuum of complex and sequential chronic inflammatory reactions tunnels into TGFβ, Smad, NF-κB, and MAPK signaling cascades [2–12].

Silicone is the most widely used implant material in routine medical practice, despite side effects, such as the formation of capsular contracture causing pain, a distinguishing aesthetic result, and impairment of implant function [13–16]. No matter how noninvasive, surgical implantation of foreign material causes injury that can initiate the fibrotic response [17, 18].

 doi:10.20944/preprints202212.0004.v1

During the last 15 years, we intensively investigated silicone breast implant-induced types of fibrosis with the objective of fundamental and clinical research [11, 19–23]. After any injury, the body goes through inflammation, matrix formation, and fiber rearrangement [11]; however, if the infection is associated with the biomaterial, the degree of fibrosis will increase dramatically[18]. We consider silicone mammary implants (SMIs) a paradigmatic example of foreign body-induced fibrotic diseases [11, 21, 22], and our findings are as well relevant for fibrotic complications in carriers of other active (cardiac pacemakers, insulin pumps, etc.) and passive (drainages, catheters, medical tubing, etc.) silicone-based devices [13, 21, 24–28]. Our generated data have clearly shown that the earliest stage of fibrosis always includes an inflammatory phase which is characterized by cells of the innate and adaptive immune system [11, 19, 21–23].

Generally, fibrosis is perceived as a reparative or reactive process [11], mainly due to the proliferation and activation of fibroblasts and myofibroblasts. Innate immune cells, such as neutrophils (during bacterial infections), eosinophils (during parasitic infections), monocytes/macrophages, mast cells, and natural killer/natural killer T (NK/NKT) cells are found in the injured tissue. Infections or injuries resulting in inflammation, initiate minor shifts in tissue homeostasis leading to migration and accumulation of inflammatory cells in the profibrotic environment inducing profibrotic signaling molecules and accelerating the development of fibrosis [11, 29] *per se.* Among these cells, macrophages, neutrophils, and mast cells are considered to be the major players in innate immune response, i.e., phagocytosis of tissue debris, dead cells, and any foreign organisms or materials, leading to fibrosis [30]. Upon macrophage activation, T cells migrate to the injury site, infiltrate the connective tissue, and release profibrotic cytokines and inflammatory mediators that stimulate/activate fibroblasts (and other cells) to transdifferentiate into α-smooth muscle actin (SMA)-expressing myofibroblasts [31–34]. If activation of myofibroblasts persists, due to insufficient elimination of the initial inflammatory stimulus (e.g., damaged tissue, foreign organisms, or foreign materials), an overproduction of ECM proteins would lead to the formation of collagen-I-rich (III > I) fibrous tissue, and ECM- degrading enzymes (such as metalloproteinases, MMPs) influence subsequent wound healing and fibrotic responses by leaving an irreversible scar that impairs the function of the organ or tissue [35, 36].

Medical device performance and biocompatibility are both directly related to unwanted side effects such as foreign body response, inflammation, and cell adhesion [26]. Silicone is a sticky and viscous material and can bind non-specifically to blood proteins[37]. When implants are inserted and come into contact with the leakage of blood at the wound site, blood biomaterial interactions emphasize protein absorption to the surface of biomaterials[38]. The adverse reaction to the adhesive proteome reflects in the activation of coagulation and leukocytes that produce inflammation, adhesion, and the activation of platelets[38, 39]. Moreover, inflammatory reactions to silicone elastomer particulate debris[40], in specific particle shedding from breast implants [41], have been demonstrated. In particular, macrophages and foreign body giant cells (FBGCs) take up silicone [42–44]. Together with neutrophils, mast cells, and fibroblasts, these cells have all been implicated in sensing the biomaterial and in producing signals that may alter fibrotic responses [25, 42].

Protein adsorption to the surface of silicon mammary implants (SMI) was investigated to date, yet either by incubation with serum proteins [19, 20, 45, 46] or post-operative by stripping off the proteome, in rats, after implant removal. However, none was performed under controlled clinical conditions as a periodical sampling intra-individually in breast cancer patients, from the acute wound first five days – and early-stage fibrosis app.8 months post-implantation.

Of note, the serum is not the only origin of foreign body response towards implants. Tissue injury, after surgical insertion of SMI, immediately activates the innate immune system setting in motion a local inflammatory response and proinflammatory mediation that includes the recruitment of inflammatory cells from the circulation [11, 29].

 doi:10.20944/preprints202212.0004.v1

Nowadays, wound fluid is commonly used for protein profiling and analysis. However, the method of sample collection used is an integral step in the research process [47, 48]. For untargeted proteomics and biomarker discovery studies, identification and measurement of large protein numbers simultaneously by mass spectrometry is favored, yet rare in implant-immunoreactivity research[49].

To date, there is no existing study of SMI-adsorbed immunoreactive proteome, from the acute wound after tissue injury, to implant encapsulation and early-stage fibrosis due to chronic inflammation. Based on the idea that apart from silicone particulate shedding, wound protein surface adsorption represents a long-term inflammatory trigger, solely markers from serum post-op may not aid in the precise molecular diagnosis or even as a predictor of performance. Therefore, we sought to identify comprehensive and distinctive marker profiles of the FBR against SMI in the acute wound milieu and later, associated with the implant surface 6-8 months after surgery. In this context, we applied a functional proteomic approach to the analysis of plasma (pre-op) as well as wound bed fluid (1-5 days post-op) and tissue expander surface-adsorbed and adhered proteome (6-8 months post-op) from breast cancer patients, undergoing simultaneously prophylactic NSME and tissue expander (inflatable implant)-based breast reconstruction. To achieve the highest possible biological significance, we, intraoperatively compared two tissue expanders with varying topography: (i) the conventionally used tissue expander at our Department- the CPX® 4 (roughness radius: 60µM Ra; Mentor) and (ii) the novel, surface-roughness reduced device SmoothSilk® (roughness: 4µM Ra; Motiva) to determine the common global SMI-adhesive proteome, adhered to both expanders in all tested subjects, though independent of silicon chemistry [50] or surface roughness [22, 51]. To track the dynamics of protein expression of immediate inflammatory response and wound healing mechanisms in the acute wound post-op we used a Tandem Mass Tag TMT-based quantitative proteomic approach. To identify potential biomarkers for early detection of early-stage fibrosis we stripped the device-associated proteome from the surface, after the tissue expanders have been exchanged with definite implants in a second operation, 6-8 months post-implantation. The set was compared with the acute wound proteome and analyzed for candidates that were associated long-term with the device surface. These results are the first to provide relevant information and insight into the aberrant progression of wound healing into fibrosis in real-time, *in-vivo.* Moreover, we provide relevant information contributing to the discovery of novel late-stage candidate biomarkers of the disease and potential therapeutic targets, providing a foundation that helps to understand the causative relation between silicone mammary implants and the autoimmune response of the immune system.

2. Materials and Methods

Study population

This study included a total of 7 female patients, who were undergoing simultaneous prophylactic bilateral nipple-sparing mastectomy (NSME) and tissue expander-based breast reconstruction. Informed consent for photo documentation, the operation, sample collection, and anonymized evaluation and publication of data was obtained in written form from all patients after confirmation of all in-and exclusion criteria (Table 1).

Table 1. Inclusion and exclusion criteria for the Expander-Immunology trial.

Preprints (www.preprints.org) | NOT PEER-REVIEWED | Posted: 1 December 2022 doi:10.20944/preprints202212.0004.v1

	Inclusion criteria
1	Female sex
2	Age > 18 years
3	High-risk family history for breast and/or ovarian cancer and/or BRCA1/2 gene mutation carrier
4	Planned bilateral mastectomy with simultaneous breast reconstruction
5	Signed Informed consent form.

	Exclusion criteria
1	Sever coagulation disorder, representing a potential contraindication for the elective surgery
2	Rheumatic disease accompanied by obligatory intake of immunomodulating therapeutic agents
3	Severe renal functional disorder: renal insufficiency status IV or V (estimated glomerular filtration rate (GFR) < 30ml/min)
4	Active hematological or oncological disease
5	HIV-Infection
6	Hepatitis-Infection
7	Pregnancy or breast-feeding
8	Intake of anti-inflammatory drugs
9	Carrier of silicone implants (e.g. gastric banding, mammary implants)

Patient demographics including age, body mass index (BMI) and breast size cup, breast symmetry, previous scars in the breast area, comorbidities (chronic diseases, allergies, therapeutics), dominant hand, smoking habits, profession (manual labor/ office job) and physical training habits as well as duration were documented. All donor biological samples (blood, wound bed fluid, and removed tissue expander) and information were obtained with the informed written consent of the participants and in accordance with: (i) the regulations of the relevant clinical research ethics committee as well as (ii) the Declaration of Helsinki and with (iii) The European Union Medical Device Regulation (§ 40 section 3 Medical Devices Act). Therefore 70 WBF samples (7 patients x 5 days post-op x 2 tissue expander types) and 14 tissue expander surface strips (7 patients x 2 expanders) were evaluated.

Study design

This monocentric, randomized, double-blind controlled clinical study was approved by the Institutional Ethical Committee of the Medical University Innsbruck, Austria (protocol code 1325/2019, 23 January 2020) and the Austrian Federal Office for Safety in Health Care (approval number; 13340962). To avoid detection of a device-exclusive immune reaction and to analyze a general SMI-associated host response, we chose to implant two tissue expanders, both composed of a poly(dimethyl siloxane) ("PDMS") elastomer shell, with varying surface topographies. We evaluated a total of 7 patients, who received either the routinely used expander Mentor CPX™4 (termed SMIb) or the novel Motiva Smooth-Silk® with reduced surface topography roughness (termed SMIa), randomized to left or right breast after prophylactic bilateral NSME (Figure 1). The patient and laboratory expert were double-blinded. Matching was performed intra-individual and conducted according to the implanted tissue expander. The inflatable tissue expanders were exchanged for definite implants in a second surgery, 6 to 8 months post-implantation.

Biological sample collection

Biological sample collection of wound bed fluid was performed daily from day 1 to 5 after expander implantation. The blood draw was performed along with anesthesia. Wound drains from patients undergoing expander-based reconstruction were left *in situ* postoperatively as part of the surgical procedure and wound bed fluid (termed WBF) was collected under sterile conditions in sterile flasks on RT. For the first 24 hours, no vacuum was applied to the drains, however right after, the drains were left *in situ* with a vacuum till removal. Flasks containing WBF were removed every 24h, for the duration of 24h-120h hours (drains after total collection time; 120h) postoperatively and WBF was transported to the cell culture in our research laboratory. To obtain proteinaceous WBF,

 doi:10.20944/preprints202212.0004.v1

we gradient-separated the drain fluid by stratification on Ficoll-Paque® (Cytivia) to remove the cellular fraction. The WBF was then sterilized by passing it through a 0.1µM and subsequently 0.07µm syringe filter to remove all cells, human and microbial. The proteinaceous fraction was frozen at -80°C for further processing.

Expander exchange with definite implants was performed during re-operation between 6 to 8 months after initial expander implantation. Removed tissue expanders were placed immediately after withdrawal into sterile boxes and frozen as well as stored at -80°C before transport to the research laboratory.

Sample preparation of wound bed fluid and serum samples for TMT-based quantitative proteomic approach

a. Immunoaffinity Depletion of High Abundant Plasma Proteins

Wound bed fluid and serum samples were subjected to immunoaffinity depletion of 14 highly abundant plasma proteins using the Multiple Affinity Removal Spin Cartridge, MARS Hu-14 (P/N: 5188-6560, Agilent Technologies). Depletion was performed according to the manufacturer's instructions. Starting material was a 30µl sample that was diluted to 600µl with Buffer A (P/N: 5185-5987, Agilent Technologies) and processed in three successive runs on the cartridge using 200µl each.

b. Protein reduction and alkylation

The proteins in 500µl of flow-through were reduced by adding 50µl 100mM dithiothreitol in Hepes-buffer (100mM Hepes, pH8.5, 10mM CaCl2) followed by incubation at 56°C for 30min. Free cysteines were alkylated by adding 50µl 550mM iodoacetamide in Hepes-buffer followed by agitation at room temperature for 20min in the dark.

c. Chloroform/methanol precipitation

Proteins were buffer exchanged by chloroform/methanol precipitation[52] In brief, a 600µl depleted sample was added to 600µl methanol and 150µl Chloroform, vortexed, and centrifuged at 15,000g for 10 min. The upper phase was discarded without disturbing the protein precipitate between the phases. Another 600µl methanol was added, vortexed and the mixture was centrifuged as before. The supernatant was discarded and the proteins in the pellet were dissolved in 95µl Hepes-buffer. Total protein concentrations were determined according to Bradford (ROTI-Nanoquant assay, P/N: K880.3, Carl Roth GmbH).

d. In-solution protein digestion and TMT-labeling

Samples were digested with 1µg of trypsin (Sequencing Grade Modified Trypsin, P/N: V5111, Promega) overnight at 37 °C under agitation. Thereafter, one-sixth of every sample was withdrawn and pooled to obtain an internal reference sample. TMT 6plex labeling was performed according to the manufacturer's instructions. In brief, samples were lyophilized to 25µl and labeled individually with 10,3µl TMT 6plex labeling. The reaction was incubated for 1 hour at room temperature, quenched with 55µl ammoniumbicarbonate buffer (100mM, pH 8.0) for 10min, and acidified with 10µl 10% formic acid. Samples were combined to have the internal reference sample and all 5 wound bed fluid samples collected at different time points from one patient and one implant side present in one pooled sample. Serum samples from different patients were pooled together with an internal reference sample. Pools were lyophilized to 30µl and subjected to high pH fractionation using Pierce High pH Reversed-Phase Peptide Fractionation Kit (P/N: 84868).

Sample preparation for* label-free quantitative proteomic analysis of *adsorbed proteins to tissue expander surface

a. Excision of tissue expander slices

 doi:10.20944/preprints202212.0004.v1

To analyze proteins attached to the surface of the tissue expander, 1cm² slice were excised from frozen expanders using a scalpel. The silicon slices were transferred to 500µl low binding tubes with the surface directed inwards. Expander slices were washed with 200µl PBS for 10min by agitation at room temperature. The supernatant was removed and the slices were subjected to protein digestion. Three technical replicates were performed per tissue expander.

b. Protein reduction, digestion, and alkylation

The proteins on the silicone slices were reduced by adding 200µl 10mM dithiothreitol in ABC-buffer (100mM Ammonium-bicarbonate, pH 8.0) followed by incubation at room temperature for 1h. For protein digestion, 2µg of trypsin was added and the reaction was agitated overnight at 37 °C. Alkylation of free cysteines was performed by adding 20µl 550mM iodoacetamide in ABC-buffer 20min in the dark. Supernatants were transferred to clean low-binding tubes followed by desalting with C18 Tips (Pierce C18 Spin Tips, P/N: 87784, Thermo). Desalted peptides were dried and stored at −20 °C.

Liquid chromatography coupled to tandem mass spectrometry (nanoLC-MS/MS)

Peptide digests were analyzed using an UltiMate 3000 nano-HPLC system coupled to a Q Exactive Plus mass spectrometer (Thermo Scientific) equipped with a Nanospray Flex ionization source as described previously (2). In brief, peptides were separated on a homemade column (100µm i.d. x 17cm length) packed with 2.4µm C18 material (Reprosil, Dr. A. Maisch HPLC GmbH). Solvents for nano-HPLC were 0.1% formic acid (solvent A) and 0.1% formic acid in 85% acetonitrile (solvent B). The total gradient time was 82min at a flow rate of 300nL/min. The 20 most abundant peptides in the survey scan were selected for MS fragmentation. The isolation window was set to 1.6 m/z. Survey full scan MS spectra were acquired from 300 to 1750 m/z at a resolution of 60 000. Peptides were fragmented by HCD with normalized collision energy set to 28 for tissue expander samples and 32 for TMT-labeled wound bed fluid samples, respectively.

Database search

The MS data files were processed using Proteome Discoverer version 2.2 (Thermo Scientific). MS/MS spectra were searched by the Sequest HT engine against a Uniprot human reference proteome database (last modified 02/02/2022). The search parameters were as follows: Enzyme specificity was set to trypsin with two missed cleavages being allowed. Fixed modification was carbamidomethyl on cysteine; variable modifications were oxidation of methionine and acetylation and/or methionine loss of the protein N-terminus. Precursor mass tolerance was set to 10 ppm; fragment mass tolerance was 20 mmu. Maximum false discovery rate (FDR) for protein and peptide identification was set to 1%. For label-free quantification of tissue expander samples, the Minora Feature Detector node was set to high confidence PSM (peptide spectrum matches) only with at least two isotopic peaks present in the isotope pattern. Retention time alignment was performed at a maximum retention time shift of 10 min and a mass tolerance of 10 ppm. For quantitation of TMT-labeled wound bed fluid samples, the protein fold changes were calculated based on TMT reporter ion intensities present in MS2 scans (m/z 126, 127, 128, 129, 130, and 131). The reporter ion intensities were extracted using the default software settings: Only peptides that were unique to a given protein or protein group were considered for quantitation. Fragment ion tolerance was set to 20 ppm for the most confident centroid peak and the co-isolation threshold was set to 50%.

The mass spectrometry proteomics data have been deposited to the ProteomeXchange Consortium (http://proteomecentral.proteomexchange.org) via the iProX partner repository with the dataset identifier PXD00000 and are publicly available as of the date of publication.

 doi:10.20944/preprints202212.0004.v1

Quantification and statistical data analysis

a. Identification, Characterization, and Quantification of common wound bed proteome

Obtained data from plasma and wound bed fluid specimens were log2 transformed and analyzed for a common set of proteins associated with both devices in the acute wound as well as interaction with the plasma proteome by *Interactivenn* [53]. Data were visualized by principal component analysis with the *ClustVis* tool [54]. In the latter, unit variance scaling was applied to rows and SVD with imputation used, to calculate principal components. Identified common proteins to both devices were tested for enriched Gene Ontology (biological process, cellular compartment, molecular function) as well as Kyoto Encyclopedia of Genes and Genomes (KEGG) pathway terms by Shiny GO software (version 0.76.3) [55]. Significance was tested with a two-sample test with a false discovery rate according to Benjamini-Hochberg set to 0.05. The Search Tool for the Retrieval of Interacting Genes/Proteins (STRING v 11.5) database of physical and functional interactions was used to analyze the protein-protein interaction (PPI) of selected proteins and clusters defined by kmeans (k=4).

Statistical data analysis of the common wound proteome was carried out with GraphPad Prism (version 9.4.1). Mean values and standard deviations were calculated for each experimental condition or type of sample. p-values between samples were calculated by unpaired t-test per protein, with individual variances computed for each comparison, combined with the two-stage linear step-up procedure of Benjamini, Krieger, and Yekutieli. Significance was tested with a two-stage set-up method with a false discovery rate set to 0.01. For visualization by volcano plots, the l2fc value was plotted against -lg10p-value by Manhattan distance in the VolcaNoseR web app [56]. Proteins were regarded as being differentially expressed when meeting the criteria $l2fc \geq \pm 1.5$ and adjusted p-value ≤ 0.01. Heatmaps were generated using the ClustVis [54]tool. Generation of tables was performed with Microsoft Excel 2018 (Microsoft Corporation). Generation of correlation plots was performed using GraphPad Prism (version 9.4.1).

b. Identification and Characterization of common adsorbed wound bed proteome on SMI surface

Obtained abundances from adhesive SMI proteome specimens were analyzed for a common set of proteins adsorbed to both devices by *Interactivenn* [53]. Data were visualized by principal component analysis with the *ClustVis* tool [54]. Identified common adsorbed proteins to both devices were submitted to Gene Ontology (biological process, cellular compartment, molecular function) as well as Kyoto Encyclopedia of Genes and Genomes (KEGG) pathway analysis by Shiny GO software (version 0.76.3) [55]. Functional categories with an adjusted p-value < 0.05 (Benjamini-Hochberg) were defined as significantly enriched. Heatmaps were generated using the ClustVis [54]tool. Generation of tables was performed with Microsoft Excel 2018 (Microsoft Corporation). Generation of correlation plots was performed using GraphPad Prism (version 9.4.1).

The statistical details of experiments are presented in the relevant figure legends. A p-value of < 0.05 was considered significant.

Significance: * $p < 0.05$/** $p < 0.01$/*** $p < 0.001$/**** $p < 0.0001$/ns = not significant.

3. Results

3.1. Ethics statement

All donor biological samples (blood, wound bed fluid, and removed tissue expander) and information were obtained with the informed written consent of the participants (EC approval number 1325/2019) and in accordance with § 40 section 3 Medical Devices Act (Austrian Federal Office for Safety in Health Care approval number; 13340962). This study was approved by the Ethics Committee of the Medical University of Innsbruck and the Austrian Federal Office for Safety in Health Care.

Preprints (www.preprints.org) | NOT PEER-REVIEWED | Posted: 1 December 2022 doi:10.20944/preprints202212.0004.v1

3.2. Patient characteristics

Seven female patients undergoing bilateral prophylactic mastectomy and simultaneous tissue expander-based breast reconstruction, due to high-risk hereditary predisposition and/or confirmed *Brca1+/Brca2+* gene mutation, were enrolled in the study (Figure 1a). To avoid detection of a device-exclusive immune reaction and to analyze a general SMI-associated host response, we chose to implant two tissue expanders, both made out of a poly(dimethyl siloxane) ("PDMS") elastomer shell, with varying surface topographies. All patients received both types of breast tissue expanders, the routinely used CPX®4 breast expanders (MENTOR®, USA: surface roughness: ~ 60 µM Ra; from here referred to as **SMIb**), and the novel surface-roughness reduced SmoothSilk® breast expanders (Motiva Flora®, Establishment Labs, Costa Rica: surface roughness: ~ 4µM Ra; from here referred to as **SMIa**) randomized to the left or right breast after bilateral prophylactic NSME (Figure 1b, c).

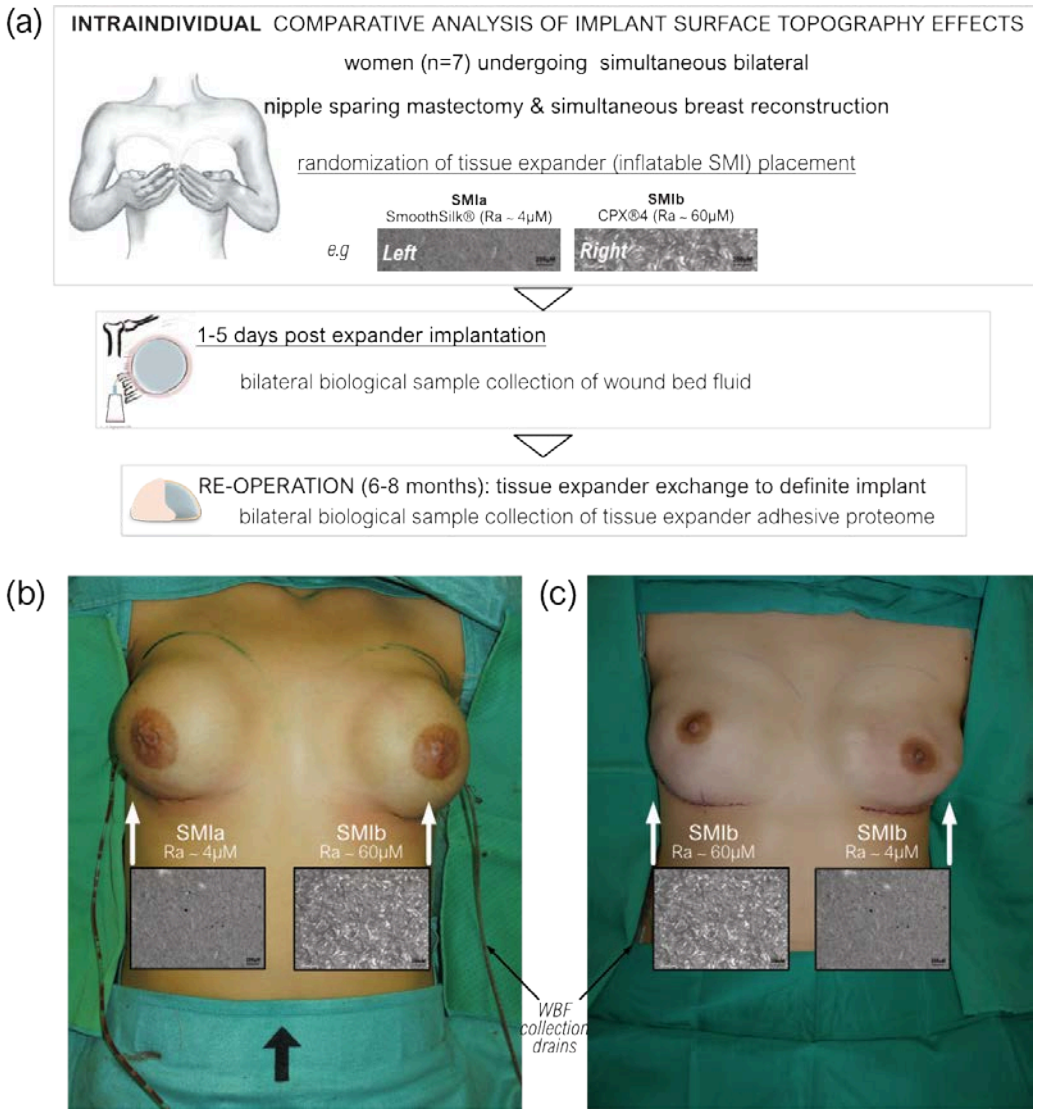

Figure 1. Standardized intra-operative photo documentation of a bilateral tissue expander-based breast reconstruction. **(a)** Each patient received both types of expanders, the novel surface-roughness reduced SmoothSilk® breast expanders (Motiva Flora®, Establishment Labs, Costa Rica: surface roughness ~ 4µM Ra; termed **SMIa**) and the routinely used CPX®4 breast expanders (MENTOR®, USA: surface roughness ~ 60 µM Ra; termed **SMIb**), randomized to the left or right breast after bilateral prophylactic NSME. **(b)** Patient 003; Right: SMIa (SmoothSilk®), Left: SMIb (CPX®4), **(c)** Patient 001; Right: SMIb (CPX®4), Left: SMIa (SmoothSilk®).

Preprints (www.preprints.org) | NOT PEER-REVIEWED | Posted: 1 December 2022 doi:10.20944/preprints202212.0004.v1

Biological sample collection of wound bed fluid was performed daily from day 1 to 5 after tissue expander implantation (wound collection drains; Figure 1b, c). After 6 to 8 months (mean duration ±SD: 6.82 ±SD 0.86 months), during re-operation, the tissue expanders were exchanged with definite implants. Due to the intraindividual comparison of tissue expanders no matching of patient groups was done, comparative analysis was based on tissue expander surface roughness as presented in Table 2. There were no significant differences in patient characteristics, mastectomy weight, implant position (prepectoral, reconstruction volume, and intraoperative filling between the two differently textured devices (Table 2). Biological sample collection by stripping the expander surface was performed immediately after the second surgery - expander removal and exchange with a definite implant.

Table 2. Intraindividual statistical comparison of analytical groups.

surface roughness	SMIa Ra ~ 4 µM		SMIb Ra ~ 60 µM		
	Mean	(±std)	Mean	(±std)	*p value*
age (y)	35.2	11.4	35.2	11.4	intraindividual comparison >0.9999
weight (kg)	71.4	24.5	71.4	24.5	
size (cm)	168.6	10.5	168.6	10.5	
BMI	25.1	6.7	25.1	6.7	
Bilateral prophylactic NSME resection weight [g]					
left breast	434.9	404.0	436.9	454.0	0.993196
right breast	334.2	257.5	337.9	174.4	0.975407
Prepectoral reconstruction volume [cc]					
left breast	405.5	156.3	392.6	151.8	0.877595
right breast	360.8	151.1	352.7	150.0	0.920737
Intra-operative filling	254.7	169.4	254.7	169.4	>0.9999

3.3. The workflow of proteomic analysis

We used a mass spectrometry approach based on Tandem Mass Tags (TMT) to quantify the common wound proteome formed around silicone breast tissue expanders (*SMIa*: SmoothSilk® silicone mammary tissue expander (implant); surface roughness 4µM and *SMIb*: CPX4 silicone mammary tissue expander (implant); surface roughness 60µM) 1 to 5 days. *TMT* are isobaric chemical tags that provide multiplexing capabilities for the relative quantification of proteomics samples.

As described in *Material and Methods*, every patient received both expanders, with applied randomized body site of implantation (Figure 1). Biological sample collection of wound bed fluid was performed from day 1 to 5 after expander implantation, the blood draws during hospital routine, namely during general anesthesia (intraoperatively), and expander surface stripping after removal of devices in re-operation between 24 to 28 weeks after initial expander implantation. A label-free approach was applied to investigate the adhesion of wound proteome on the expander surface. A brief description of the experimental workflow of proteomics studies is shown in Figure 2, as explained in detail in *Methods*. In brief, we acquired nanoLC-MS data on an FT mass spectrometer. The raw mass spectrometry files (MS) were analyzed and searched in the UniProt [57] human protein database using the ProteomeDiscoverer platform (Thermo Scientific).

The proteins in the wound fluid and plasma samples were enzymatically digested and the resulting peptides were labeled with TMT reagents (Figure 2A). In order to be able to compare the samples or subjects with one another, 1/6 of each digest was pooled and labeled separately. This pool served as the standard and was used for normalization. Subsequently, wound bed fluid and plasma samples were combined into the TMT 6-plex sets of 5 samples one patient/side (1x subject; 5 samples (D1-D5); 1x tissue expander roughness type) and 1 standard each (e.g., patient 1, WBF formed around 60µM CPX4 expander from day 1-5 post-surgery). The plasmas were assessed in a separate TMT 6-plex set. In order to increase protein identification numbers, the pooled samples were

Preprints (www.preprints.org) | NOT PEER-REVIEWED | Posted: 1 December 2022 doi:10.20944/preprints202212.0004.v1

chromatographically separated into 8 fractions using a high-pH column prior to the nanoLC-MS analysis.

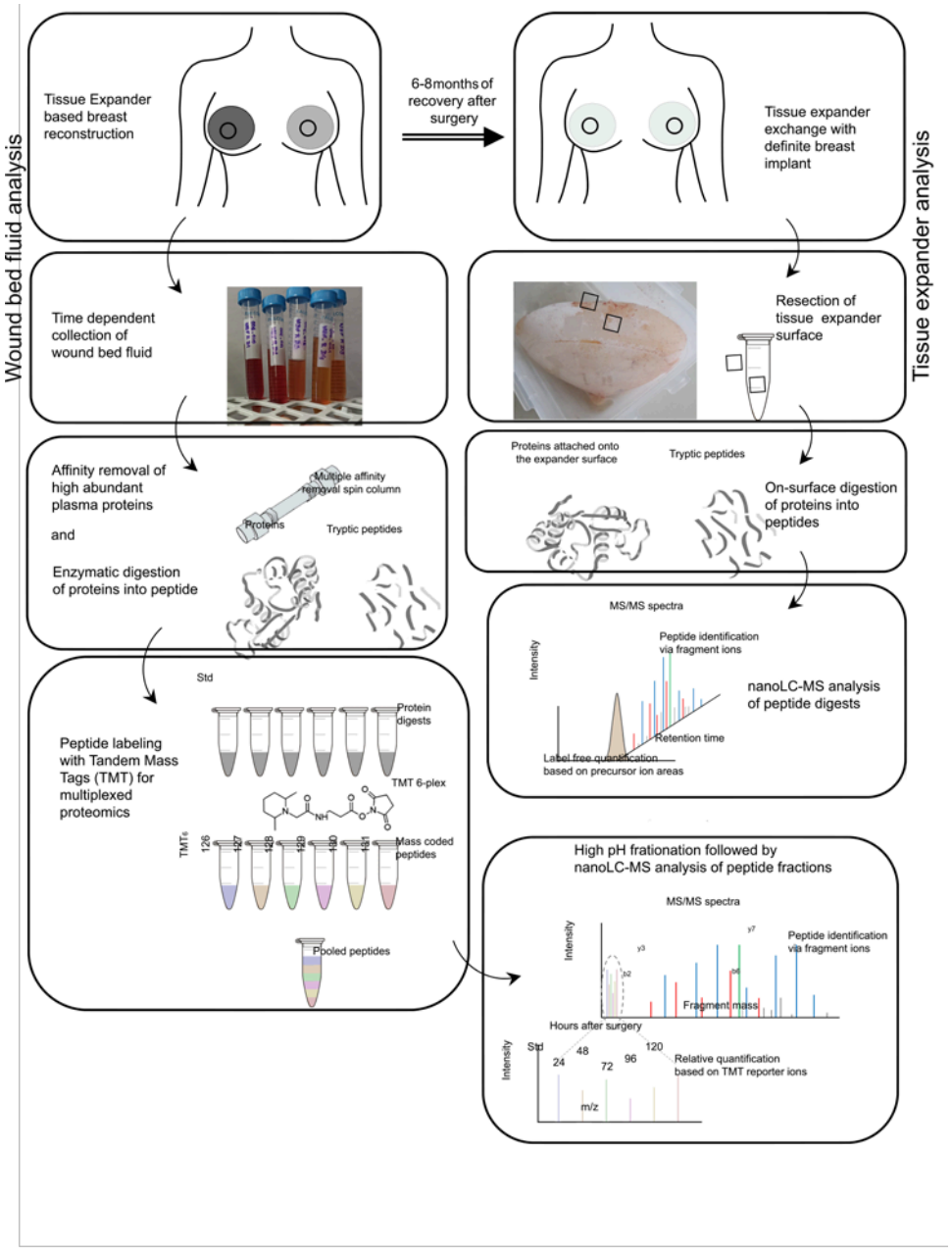

Figure 2. Experimental design of proteomic analyses. **(a)** wound bed fluid analysis. **(b)** tissue expander analysis.

After removal of devices in re-operation between 24 to 28 weeks after initial expander implantation, 6 pieces of approx. 1cm² were removed from each SMI surface (SMIa and SMIb) and transferred into separate test tubes (Figure 2B). The proteins adhering to the silicone surface were then digested, with 3 pieces washed with PBS beforehand. From each of the 6 samples, 5% were then analyzed by nanoLC-MS. The quantification is based on the integrated peak areas per peptide, which are summed up at the protein level and result in a protein abundance.

Preprints (www.preprints.org) | NOT PEER-REVIEWED | Posted: 1 December 2022 doi:10.20944/preprints202212.0004.v1

The mass spectrometry proteomics data have been deposited to the ProteomeXchange Consortium (http://proteomecentral.proteomexchange.org) via the iProX partner repository with the data identifier PXD00000.

3.4. Quantification and data integrity of intraindividual comparative proteomic profiling in plasma, wound, and SMI-adhesive proteome

The samples of wound bed fluid formed around expanders and plasma were comparatively analyzed by the TMT-based proteomics method to determine the proteins which may be related to the molecular mechanisms or triggers of immediate inflammatory response towards silicone implantation in the first five days after surgery. We obtained a high coefficient of correlation (R2) value for the sample TMT abundance ratios compared to the standard (Supplementary Figure 1). Figure 3C presents the box plot for the log2 values of the TMT abundance ratios, corresponding to the wound bed fluid samples (n=7; in triplicates) of each group (n=3; plasma, SMIa, SMIb) indicating that the interquartile range and median are similar between the biological replicates (n=7) of each group (Figure 3C-D), showing the consistency of the values obtained in the LC-MS/MS measurements.

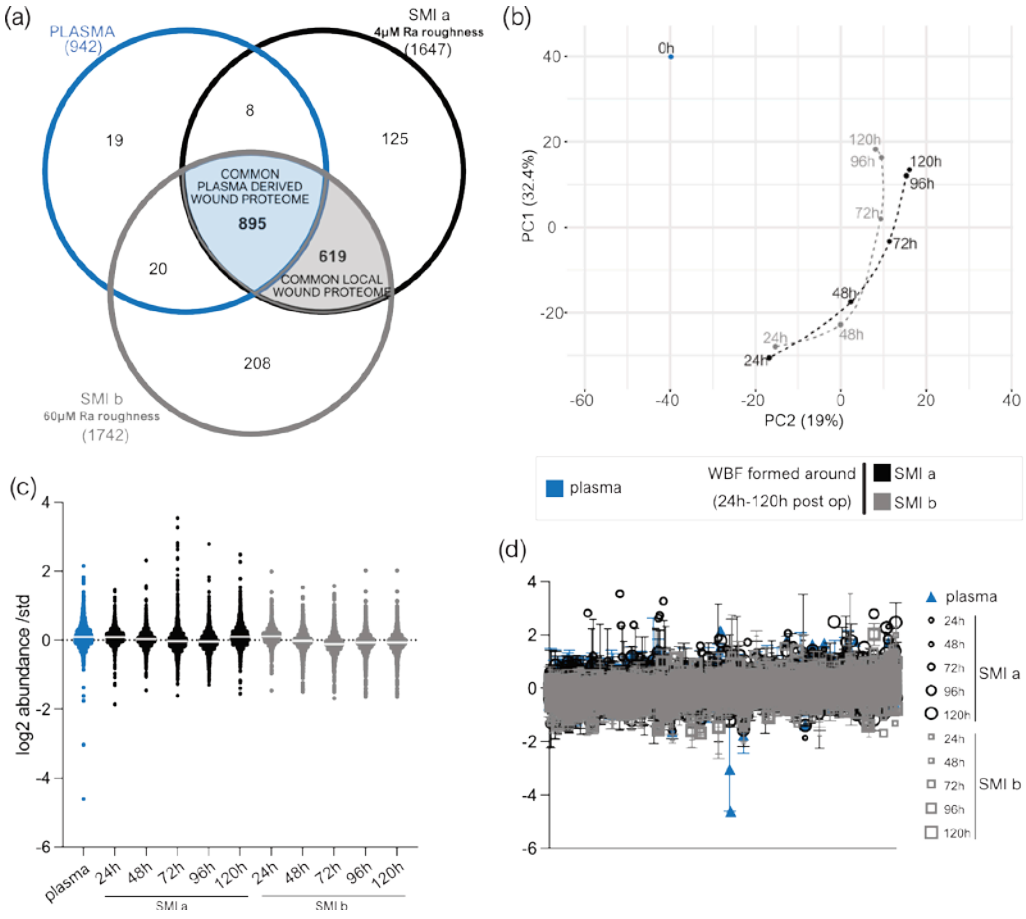

Figure 3. LC-MS/MS reproducibility and distribution of proteins identified. **(a)** Venn diagram showing the distribution of proteins in the collected plasma and wound bed fluid formed intraindividual around tissue expanders with 4µM (SmoothSilk®) and 60µM (CPX®4) surface roughness. **(b)** PCA was obtained with a median log2 abundance of the differential proteins found in all samples. **(c)** Scatter plot of median results with interquartile range obtained by wound proteome analysis on 7 patients, with 2 different silicone tissue expanders implanted, in plasma and wound bed fluid formed around the devices 1 to 5 days post-surgery. **(d)** Row statistics plot of all replicates with interleaved symbols (at mean). The level for statistical significance was set at $p^{ns} \geq 0.05$, $p^{*} < 0.05$,

 doi:10.20944/preprints202212.0004.v1

p**<0.002, p***<0.0002, and p****<0.0001, for all statistical tests. (inter- and intra-individual comparison; n=7)

We adopted label-free quantitative proteomic analysis to investigate and identify which immediate foreign body response proteins from the wound environment potentially adhere to the SMI surface - and chronically trigger excessive ECM turnover, resulting in fibrotic capsule formation.

Principal component analysis revealed a high interindividual sample variation, by principal component 1 and principal component 2 that explain 43.2% and 21.1% of the total variance, respectively (Supplementary materials, Figure S2b). The distribution of protein abundance ratio displayed in Supplementary Figure S2b obeyed normal distribution and revealed a coefficient of correlation (R2) between the individual patient samples abundance ratios compared for both SMI (Supplementary materials, Figure 2 d-e; i-ii). Normality and Lognormality tests confirmed a lognormal data distribution, due to failing normality tests with p****> 0.0001 (Supplementary materials, Figure S2 d-e; iii).

3.5. Distribution of wound proteins identified by proteomic analysis

A total of 942 plasma proteins as well as 1514 common wound proteins were identified in the wound environment around both expanders, all matched in the UniProt_HomoSapiens database (Appendix A. additional file, Table 3). Among the identified 1514 wound proteins, we characterized 895 as common plasma-derived wound proteome (Figure 3a; light blue and Appendix A. Additional file Table 4), confirmed by its abundance in the plasma serum sample. 619 wound proteins were not found in the plasma sample, though characterized as the local wound proteome (Figure 3a; light grey and Additional File, Table 7).

PCA analysis highlighted the spatial distribution of the 11 samples (plasma; WBF around 4μM textured expander 1-5D post-op; WBF around 60μM textured expander 1-5D post-op) and revealed segregation between wound bed fluid and plasma samples and high correlation between the two differential wound bed fluids formed around SMIa and SMIb at every sampling time point (Figure 3b). In specific the temporal visualization of wound proteome differentiation over the first five days after expander implantation revealed a periodical time-dependent proteomic shift towards reduction of segregation between the plasma (Figure 3b; 0h, blue) and wound proteome (Figure 3b; 24h-120h, SMIa: black, SMIb: grey) chronologically - wound proteome composition and abundance on day 5 reflecting closer relation to pre-surgery plasma proteome.

3.6. Composition of plasma-derived wound proteome formed around silicon tissue expanders the first five days after implantation

To better understand the functions and pathways in which the proteins identified exclusively as plasma-derived wound proteome (895 proteins common to both devices) may be involved, we performed (Figure 4a) Gene Ontology (GO) and (Figure 4b) Kyoto Encyclopedia of Genes and Genomes (KEGG) pathway analysis. The GO results revealed that the proteins of the plasma-derived wound proteome are associated mainly with the inflammatory and immune cell activating BP (biological processes) such as neutrophil-mediated immunity (activation, regulation, degranulation), granulocyte and leucocyte activation, as well as regulation of exocytosis and secretion by cell (Figure 4a). However, the most representative GO biological process category was secretion, encompassing 122 proteins, followed by leucocyte activation (103 proteins), and granulocyte-, leucocyte-, neutrophil- activation as well as degranulation (Supplementary material, Table S1).

Preprints (www.preprints.org) | NOT PEER-REVIEWED | Posted: 1 December 2022 doi:10.20944/preprints202212.0004.v1

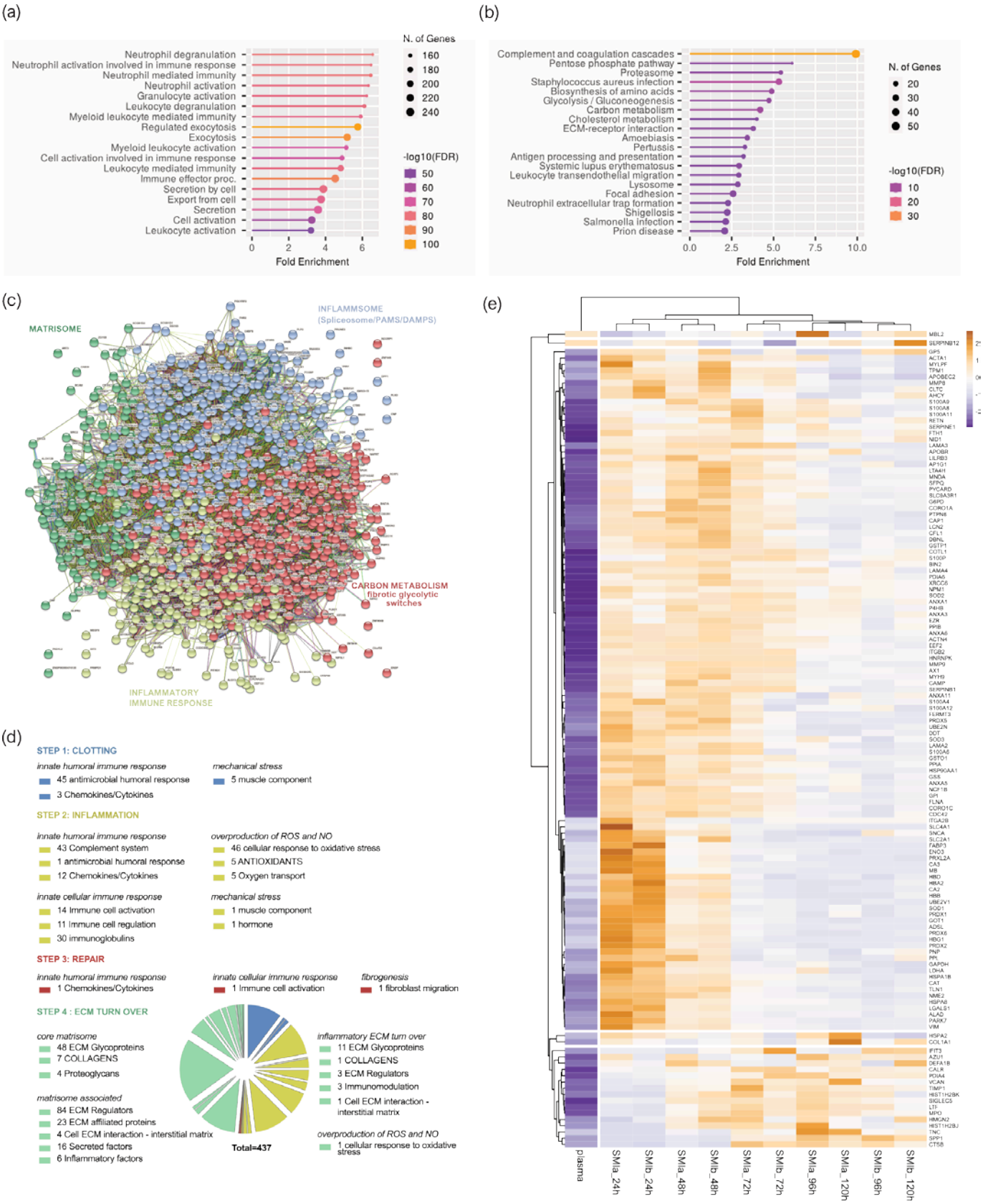

Figure 4. Plasma-derived wound proteome. **(a)** GO biological process enrichment, **(b)** KEGG pathway enrichment analysis **(c)** protein-protein interaction regulatory network by K-means clustering based on STRING database, **(d)** functional categorization in the context of tissue repair of common plasma-derived wound proteome formed around 2 different silicone tissue expanders implanted (intraindividual comparison; n=7), 1 to 5 days post-surgery. **(e)** Heatmap analysis of DEP in the plasma-derived wound proteome. *Rows:* Clustered by Manhattan distance, average method, and tightest cluster first tree ordering. Columns: Clustered by correlation

 doi:10.20944/preprints202212.0004.v1

distance, average method, and tightest cluster first tree ordering. The level for statistical significance was set at $p^{ns} \geq 0.05$, $p^{*}<0.05$, $p^{**}<0.002$, $p^{***}<0.0002$, and $p^{****}<0.0001$, for all statistical tests. (inter- and intra-individual comparison; n=7)

KEGG pathway enrichment analysis showed that the plasma-derived proteins in wound bed fluid formed around implanted tissue expanders (d1-d5) belonged to mainly complement and coagulation cascades, the proteasome, carbon metabolism, ECM- receptor interaction, metabolic pathways, phagosome, chemokine signaling pathway, spliceosome, focal adhesion, FC gamma R-mediated phagocytosis and leucocyte trans-endothelial migration (Figure 4b and Supplementary material, Table S2). The complement and coagulation cascade was the most representative pathway, with an enrichment FDR of 2.6e-48 encompassing 50 plasma-derived wound proteins, followed by immunity-related chemokine carbon metabolism and ECM-receptor interaction pathways, encompassing 29 and 20 expressed plasma-derived proteins, respectively.

Together, the GO and KEGG enriched functional annotation describe an SMI-induced hyperinflammatory response with complement and immune cell activation, a cytokine storm, and coagulopathy. To further our understanding of the immediate change in wound proteome composition in the progress of capsular fibrosis, we evaluated the interaction of the 895 proteins, using the search tool for retrieval of interacting genes/proteins STRING (V11.5; string-db-org). The analysis provided us with a PPI network consisting of 868 nodes and 15100 edges, with an average node degree of 34.8 and a local clustering coefficient of 0.1. The expected number is 5617 and a PPI enrichment p-value <1.0 e-16 (Figure 4c).

To further our understanding of the regulatory role of immediate wound proteome in the context of SMI-associated fibrosis, we applied K-means clustering and identified 4 major clusters of proteins (Figure 4c), mainly enriched in KEGG pathways, reflecting different phases of tissue damage response (Table 5; cluster 3 and 4) and tissue repair (Table 5; cluster 1 and 2).

Table 5. STRING kmeans(k=4) cluster description of plasma-derived wound proteome.

	Cluster 1	Cluster 2	Cluster 3	Cluster 4
	RED	GREEN	YELLOW	BLUE
	CARBON METABOLISM in fibrolytic switches	MATRISOME	INFLAMMATORY IMMUNE CELL RESPONSE	INFLAMMSOME
proteins	281	120	159	308
nodes	281	120	159	308
edges	3592	503	1310	4526
average node degree	25.6	8.38	16.5	29.4
local clustering coefficient	0.51	0.52	0.541	0.491
expected number of edges	1284	18	163	479
PPI enrichment p-value				
	<1.0 e-16	<1.0 e-16	<1.0 e-16	<1.0 e-16

Tissue damage response was recognized in cluster 4 (blue) which included 308 proteins mainly enriched in complement and coagulation cascades, and in cluster 2 (yellow), with 159 proteins (cluster 4; Supplementary material, Table S5) involved in FC gamma R-mediated phagocytosis and Leucocyte endothelial migration (cluster 2; Supplementary material, Table S6). Cluster 1 (red), containing 281 proteins with the most representative KEGG enrichment in the pentose phosphate pathway, glycolysis/gluconeogenesis, and carbon metabolism (cluster 1; Supplementary material, Table S7), and cluster 3 (green) united 120 proteins involved in the core matrisome and/or ECM turn over (cluster 3; Supplementary material, Table S8) were recognized as part of tissue damage repair and ECM turn-over processes.

 doi:10.20944/preprints202212.0004.v1

Among the 895 common plasma-derived wound proteins, 437 proteins were identified according to their biological role (investigated in UniProt database) as proteins involved in inflammatory excessive ECM turnover – the inflammatory matrisome. Depending on their annotated role (Uniprot), we functionally annotated these into steps of tissue repair after SMI implantation (Figure 4d: step 1. clotting, step2. inflammation, step 3. repair and fibrogenesis and step 4. ECM turn-over) More details can be found in supplementary material, Table S8.

A volcano plot was applied to delineate differential protein abundance against the corresponding *p*-value obtained (Supplementary Figure S3a). Among the 437 identified plasma-derived proteins in the wound bed, we identified in total 102 significantly differentially upregulated) over the total timespan, from day 1 to day 5 (Table 6 and Supplementary Figure S3a), common to both SMI in comparison with the plasma of patients and controls (Supplementary material, Table S9). Applied Manhattan distance clustering of samples reveals the (i) discrimination between plasma and wound proteome, (ii) the proteome composition and expression similarity around both SMI devices, and (iii) discrimination between the day of sampling post-implantation.

Again, the wound proteins attracted to both SMI from plasma showed the highest upregulation on day 1, with a gradual descent over the first 120h post-implantation (Supplementary Figure S3c).

Table 6. Numbers of inflammatory matrisome proteins in plasma-derived wound proteome after silicon device implantation.

	inflammatory matrisome class	number of common plasma derived wound proteins [a]	number of differentially expressed plasma derived wound proteins [b]	Ratio [%]
innate humoral immune response	antimicrobial humoral response	46	15	33%
	chemokines/cytokines	16	5	31%
	complement system	43	9	21%
innate cellular immune response	immune cell activation	15	5	33%
	immune cell regulation	11	8	73%
	immunoglobulins	30	0	0%
overproduction of ROS and NO	cellular response to oxidative stress	47	24	51%
	oxygen transport	5	5	100%
	antioxidants	5	5	100%
mechanical stress	muscle component	6	6	100%
	hormone	1	1	100%
core matrisome	ECM glycoproteins	59	13	22%
	collagens	8	1	13%
	proteoglycans	4	0	0%
matrisome associated	ECM regulators	87	12	14%
	ECM affiliated proteins	23	6	26%
	cell ECM interaction - interstitial matrix	5	2	40%
	secreted factors	16	9	56%
	inflammatory factors	6	2	33%
	immunomodulation	3	0	0%
	fibroblast migration	1	1	100%

[a, b] More details can be found in supplementary material, Table S8, and S9.

Among the 102 differentially expressed proteins we identified 42 proteins of the innate immune response (humoral and cellular), 34 proteins involved in the regulation of oxidative stress, 7 responders to mechanical stress, and 46 ECM proteins (Supplementary Figure S2B and Table 6). More details can be found in supplementary material, Table S8, and S9. This set of 42 innate immune response proteins was composed of 29 factors of the humoral (DAPMs, PAMPs, AMPs, splicing factors, cytokines, and chemokines, etc…) and 13 proteins involved in immune cell activation and regulation. Among them, HSPA1B, A8, and A2 *are* implicated in the development of fibrosis and HSP90AA, a regulator of fibroblast activation (Figure 4e, supplementary material, Table S8, and S9).

The set of ECM proteins was composed of 16 core matrisome proteins (13 ECM glycoproteins and 1 collagen chain) and 32 ECM-associated proteins (12 ECM regulators,

 doi:10.20944/preprints202212.0004.v1

23 ECM-affiliated proteins, 6 cell-interaction components, and 3 secreted factors). Surprisingly, we found COL1A1, COL3A1 COL1A2, COL6A1, COL6A2, and COL6A3 abundant in the wound proteome around both SMI, however, COL1A, a prominent driver of fibrosis, was the only significantly upregulated over the total 120h post-surgery (Figure 4e, supplementary material, Table S9). As expected, we identified the matrisome associated S100A protein family as part of the FBR in the wound, with S100P, S100A4, S100A6, S100A7, S100A8, S100A9, S100A11, S100A12 significantly upregulated compared with the corresponding unstimulated abundance in plasma. Conformingly, the upregulation of MMP98 and MMP9 enzymes and EMC glycoprotein Vimentin and Nidogen in the wound milieu, reflect a clear change in ECM turnover (Figure 4e, supplementary material, Table S9).

3.7. Proinflammatory mediation in local wound proteome formed around silicon tissue expanders the first five days after implantation

The plasma-derived wound proteome resembles a clear FBR toward both silicone implants in the first five days after implantation, characterized through different stages of tissue repair as an inflammatory matrisome.

In the next step, we aimed to further understand the functions of local wound proteome (Appendix A. additional file, Table 7; 619 proteins common to both devices) and how the origin (plasma or local) of FBR proteome can affect the progression from regular wound healing processes to tissue repair "gone wild" in the context of fibrosis. Again, we performed (Figure 5a) GO and (Figure 5b) KEGG pathway analysis.

Preprints (www.preprints.org) | NOT PEER-REVIEWED | Posted: 1 December 2022 doi:10.20944/preprints202212.0004.v1

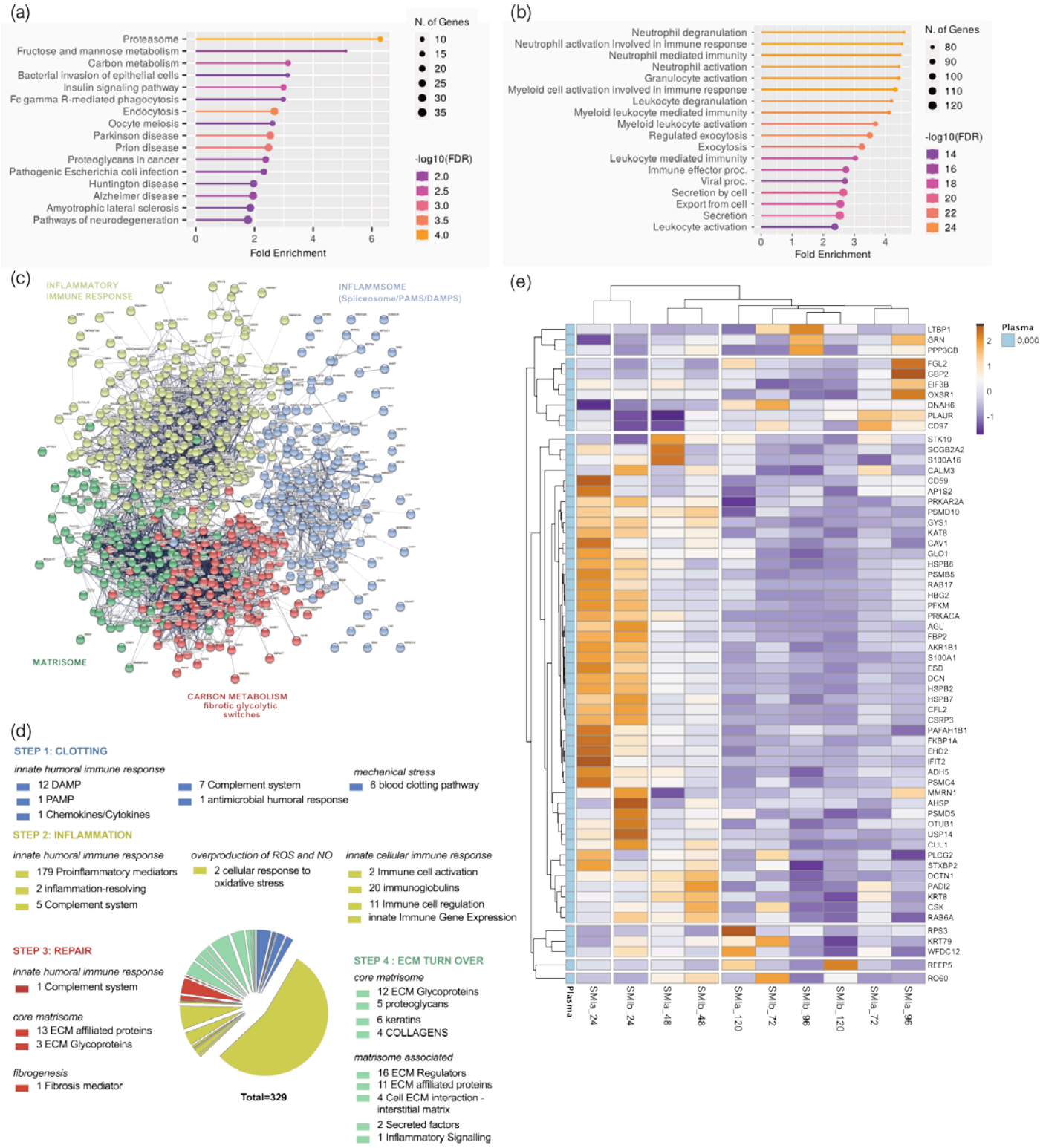

Figure 5. Local wound proteome. **(a)** GO biological process enrichment, **(b)** KEGG pathway enrichment analysis **(c)** protein-protein interaction regulatory network by K-means clustering based on STRING database, **(d)** functional categorization in the context of tissue repair of common local wound proteome formed around 2 different silicone tissue expanders implanted (intraindividual comparison; n=7), 1 to 5 days post-surgery. **(e)** Heatmap analysis of DEP in the local wound proteome. *Rows:* Clustered by Manhattan distance, average method, and tightest cluster first tree ordering. Columns: Clustered by correlation distance, average method, and tightest cluster first tree ordering. The level for statistical significance was set at $p^{ns} \geq 0.05$, p*<0.05, p**<0.002, p***<0.0002, and p****<0.0001, for all statistical tests. (inter- and intra-individual comparison; n=7)

Preprints (www.preprints.org) | NOT PEER-REVIEWED | Posted: 1 December 2022 doi:10.20944/preprints202212.0004.v1

GO results revealed that the proteins of the local proteome enrich mainly with immune cells activating BP (biological processes), corresponding to the plasma-derived wound proteome. However, KEGG pathway analysis revealed a predominant enrichment in the proteasome category (Figure 5b) but not the complement system as seen in the plasma-derived proteins (Figure 4b) in wound bed fluid formed around implanted tissue expanders (d1-d5). The STRING database was employed to construct the protein-protein interaction networks among these 619 proteins. The analysis provided us with a PPI network consisting of 601 nodes and 4341edges, with an average node degree of 14.4 and a local clustering coefficient of 0.321. The expected number is 2635 and a PPI enrichment p-value <1.0 e-16 (Figure 5c). As before we applied kmeans (k=4) clustering to the network into four main clusters described in Table 8.

Table 8. STRING kmeans cluster description of local wound proteome.

	Cluster 1	Cluster 2	Cluster 3	Cluster 4
	RED	GREEN	YELLOW	BLUE
	CARBON METABOLISM in fibrolytic switches	MATRISOME	INFLAMMATORY IMMUNE CELL RESPONSE	INFLAMMSOME
proteins	150	117	221	123
nodes	150	117	221	123
edges	306	575	967	967
average node degree	4.08	9.83	9.17	15.7
local clustering coefficient	0.394	0.531	0.38	0.515
expected number of edges	49	123	307	242
PPI enrichment p-value				
	<1.0 e-16	<1.0 e-16	<1.0 e-16	<1.0 e-16

Tissue damage response and repair were recognized and categorized, enriched in KEGG pathways comparably to plasma-derived proteome (supplementary material, Table S10-S13). Subsequently, 329 proteins were categorized as inflammatory matrisome proteins and functionally annotated into steps of tissue repair after SMI implantation (Figure 5d; step 1. clotting, step2. inflammation, step 3. repair and fibrogenesis and step 4. ECM turn-over) More details can be found in supplementary material, Table S14. Among the 329 identified local wound proteins, we identified in total 63 significantly differentially expressed (upregulated, Supplementary material, Figure S4a) over the total timespan, from day 1 to day 5 (Table 9), common to both SMI of patients and controls from day 1 to day 5 post-surgery (Supplementary material, Table S15). Corresponding to plasma-derived wound proteome, also the local wound protein samples formed clusters (Manhattan distance) in dependence on the time-point of sampling post-implantation and showed the highest upregulation on day 1, with a gradual descent over the next 4 days (Supplementary Figure S4c).

Table 9. Numbers of inflammatory matrisome proteins in local wound proteome after silicon device implantation.

 doi:10.20944/preprints202212.0004.v1

	inflammatory matrisome class	number of common local wound proteins [a]	number of differentially expressed local wound proteins [b]	Ratio [%]
innate humoral immune response	DAMP	12	0	0%
	PAMP	1	0	0%
	antimicrobial humoral response	1	1	100%
	Chemokines/Cytokines	1	0	0%
	Complement system	13	2	15%
	blood clotting pathway	6	3	50%
	Pro-inflammatory mediators	179	36	20%
	inflammation-resolving	2	0	0%
innate humoral immune response	Innate Immune Gene Expression	1	0	0%
	Immune cell activation	2	0	0%
	Immune cell regulation	11	3	27%
	immunoglobulins	20	0	0%
	cellular response to oxidative stress	2	0	0%
	Fibrosis mediator	1	0	0%
core matrisome	ECM Glycoproteins	15	1	7%
	KERATINS	6	2	33%
	COLLAGENS	4	0	0%
	Proteoglycans	5	1	20%
matrisome associated	ECM affiliated proteins	13	5	38%
	ECM Regulators	16	1	6%
	ECM affiliated proteins	11	0	0%
	Cell ECM interaction - interstitial matrix	4	1	25%
	Secreted factors	2	2	100%
	Inflammatory Signaling	1	0	0%
oncologic marker	mammaglobin A	1	1	100%

[a, b] More details can be found in supplementary material: Tables S14 and S15.

3.8. Wound proteome adsorption on SMI surfaces in the first 8 months post-implantation

SMI-associated capsular fibrosis is characterized by an excessive accumulation of the extracellular matrix as a response to different types of tissue injuries over a longer period. This FBR can be initiated by multiple and different stimuli and pathogenic factors, but mainly by the foreign body inserted, which triggers the cascade of reparation converging in molecular signals responsible for initiating and driving fibrosis. To answer the question of what part and which components of the implant encompassing immediate wound proteome serve as triggers of a long-lasting chronic inflammation we stripped the SMI-associated proteins from the tissue expander surface app. 8 months post-op, as the expanders were exchanged with definite implants.

A total of 358 proteins adhered to SMIa and 263 to the SMIb surface (Appendix A. additional files, Table 10 and Figure 6a) were identified (in all five patients tested of 7 enrolled) in the UniProt database (uniprot_HomoSapiens). PCA variance analysis has shown no proximity of samples, revealing high interindividual variation in total adhesive proteomes (Supplementary Figure S2). Among the adhered identified proteins, we identified 233 common proteins, associated with both expanders (Appendix A. additional files, Table 11 and Figure 6a).

To gain a comprehensive understanding of the biological significance of these 233, silicone surface-associated and/or adhered proteins, we conducted GO and KEGG analysis to characterize their potential functions. Our data revealed that these proteins are associated mainly with BP such as secretion, regulation of exocytosis, cell activation and protein metabolism, targeting, and localization (Figure 6b). Besides, concerning MF, these proteins are mainly involved in binding of molecules to the surface: rRNA and RNA -, protein (cadherin, unfolded proteins, integrin, actin, cell adhesion, protein-containing complex, cytoskeletal protein, and signal receptor molecule)- and lipid binding, and structural molecule activity in the context of ECM matrix structural constituent (Figure 6c). Moreover, in connection with the CC, proteins were enriched for the collagen-containing extracellular matrix, extracellular matrix, and as an external encapsulating structure, as well as secretory granule and vesicle (Figure 6d). In addition, the results obtained from the KEGG pathway enrichment analysis confirmed that these silicone surface-associated proteins are related to pathways such as ECM receptor interaction, complement, and coagulation cascades and the phagosome, 8 months after device implantation (Figure 6e). Due to the high interindividual variation of protein abundance on the silicone surfaces,

Preprints (www.preprints.org) | NOT PEER-REVIEWED | Posted: 1 December 2022 doi:10.20944/preprints202212.0004.v1

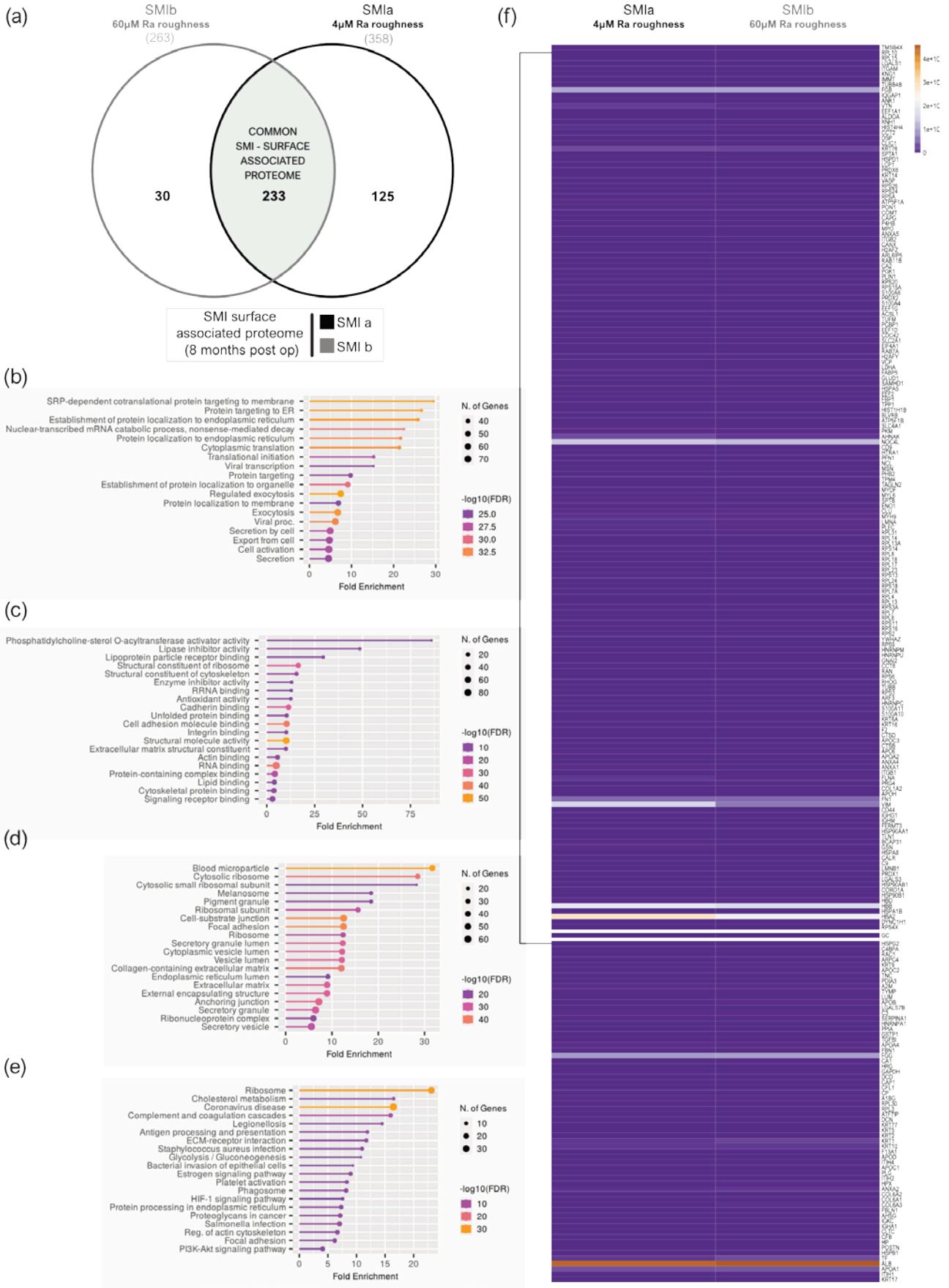

Figure 6. SMI surface-associated adhesive proteome. **(a)** Venn diagram showing the distribution of proteins associated at silicone tissue expander surface (SMIa: 4μM and SMIb 60μM surface roughness. **(b)** GO biological process enrichment, **(c)** GO molecular

Preprints (www.preprints.org) | NOT PEER-REVIEWED | Posted: 1 December 2022 doi:10.20944/preprints202212.0004.v1

function enrichment, **(d)** GO cellular component enrichment, **(e)** KEGG pathway enrichment analysis of common SMI surface-associated adhesive proteome. **(f)** Heatmap analysis of mean protein abundance of common adhesive proteome on SMIa and SMIb. *Rows:* Clustered by Manhattan distance, average method, and tightest cluster first tree ordering. Columns: no clustering applied. The level for statistical significance was set at $p^{ns} \geq 0.05$, p*<0.05, p**<0.002, p***<0.0002, and p****<0.0001, for all statistical tests. (inter- and intra-individual comparison; n=7).

we compared mean protein abundance on SMIa and SMIb and confirmed a common pattern of expression of the common adhesive proteome on both devices (Figure 6f).

3.9. From wound to early-stage fibrosis: adhesion of inflammatory matrisome to silicone surfaces

The final stage in wound healing/foreign body response to biomaterials is generally fibrosis and fibrous encapsulation of the implanted device. Finally, we aimed to investigate and identify which proteins from the acute wound environment potentially adhere to the SMI surface long-term - and chronically trigger excessive ECM turn-over 8 months post silicon device implantation.

Corresponding to the wound proteome analysis, the 233 proteins of common (to both SMI) SMI-surface associated proteome were categorized as inflammatory matrisome proteins and functionally annotated into steps of tissue repair after SMI implantation (Figure 7a-b and Supplementary material, Table S16). Among the common SMI-associated proteins we identified 3 categories: adhered proteins from plasma-derived (117 proteins; Supplementary material, Table S17) and local (17 proteins; Supplementary material, Table S18) wound proteome as well as novel SMI surface and time point (8 months post-op) exclusive proteins (67 proteins, Supplementary material, Table S19). As presented in Table 12, we found 30% of plasma-derived and 6% of local acute wound-associated inflammatory components adhered to SMI surfaces, from plasma mainly antimicrobial response agents and local proinflammatory mediation by ribosomal proteins.

Table 12. Acute wound proteome association with SMI surfaces 6-8 months post-implantation.

	inflammatory matrisome class	number of plasma derived wound proteins *d1-d5 post SMI implantation*	number of plasma derived wound proteins ***associated with SMI surface*** *6-8 months post SMI implantation*	Ratio [%]	number of local wound proteins	number of local wound proteins ***associated with SMI surface*** 6-8 months post SMI implantation	Ratio [%]
innate humoral immune response	DAMPs				1	1	100%
	antimicrobial humoral response	46	8	17%			
	chemokines/cytokines	16	3	19%			
	proinflammatory mediation (ribosomal proteins)				179	10	6%
	complement system	43	3	7%			
innate cellular immune response	immune cell activation	15	4	27%			
	immune cell regulation	11	5	45%			
	immunoglobulins	30	4	13%			
overproduction of ROS and NO	cellular response to oxidative stress	47	10	21%			
	oxygen transport	5	3	60%			
	antioxidants	5	3	60%			
mechanical stress	muscle component	4	1	25%			
	hormone	1	0	0%			
INFLAMMATORY RESPONSE		**223**	**44**	**20%**	**180**	**11**	**6%**
core matrisome	ECM glycoproteins	59	16	27%	15	1	7%
	collagens	8	4	50%	4	1	25%
	proteoglycans	4	3	75%	5	1	20%
	keratins				6	1	17%
matrisome associated	ECM regulators	87	24	28%			
	ECM affiliated proteins	23	8	35%			
	cell ECM interaction - interstitial matrix	5	3	60%			
	secreted factors	16	4	25%			
	inflammatory factors	6	0	0%			
	immunomodulation	3	3	100%			
	fibroblast migration	1	0	0%			
ECM TURN-OVER		**212**	**65**	**31%**	**30**	**4**	**13%**

a,

Among the adhered core matrisome components, we identified not only vimentin, vitronectin fibronectin, laminin, fibrillin, elastin, glycoproteins, and proteoglycans that take part in the formation of extracellular matrix (ECM) were found associated with the SMI surface but also various collagen types from plasma (Table 9; COL-1, -3, -4, -5, -6, -12, -14, -15, -18), although only COL1 and COL6 were significantly upregulated in the acute wound (Figure 7Cii). In the context of chronic progression from an acute wound to capsular fibrosis, our data reveal that molecular proinflammatory mediators such as (i) TGFß1, CD44, HSP70, and HSP90 family members as well as fibrosis drivers from (ii) core matrisome components fibronectin, vitronectin and vimentin, COL1A and COL6(A1-A3) but also (iii) secreted factors of the S100A (A4, A6, A10, and A11) family are recruited as plasma components to the wound and associate/ adhered to SMI surface (Figure 7c). COL3 was significantly upregulated only on days 3 and 4 and dropped to plasma levels

 doi:10.20944/preprints202212.0004.v1

on day 5 again (Supplementary Figure S8). At these time points, COL3 was significantly increased in comparison to COL1 (Supplementary Figure S8). Generally, the expression of these proteins periodically decreases during the first five days post-op, except TGFß1 (Figure 7c-i).

Additionally, local wound exclusive profibrotic response, HSP60, as well as MCP-1, were found among the adhered proteins (Figure 7d). Both, act directly on antigen-presenting cells (APC) and enhance T-cell activation. Importantly - we found T-complex (in form of CCT8) abundance /adhesion on the SMI surface (supplementary material, Table S18). No detection of Mammaglobin A on the SMI surface could be confirmed.

Among the 67 found exclusively 8 months post-implantation on SMI surface, we identified in total 37 proteins involved in the innate response, mainly proinflammatory and profibrotic mediating 40S/60S ribosomal proteins; the MIC complex and Macrophage capping protein. The most interesting among matrisome components was the detected CD9 antigen – the pro-fibrogenic and proinflammatory macrophage senescence factor, confirming their phagocytotic activity seen previously in GO and KEGG enrichments (Figure 6b-c).

Preprints (www.preprints.org) | NOT PEER-REVIEWED | Posted: 1 December 2022 doi:10.20944/preprints202212.0004.v1

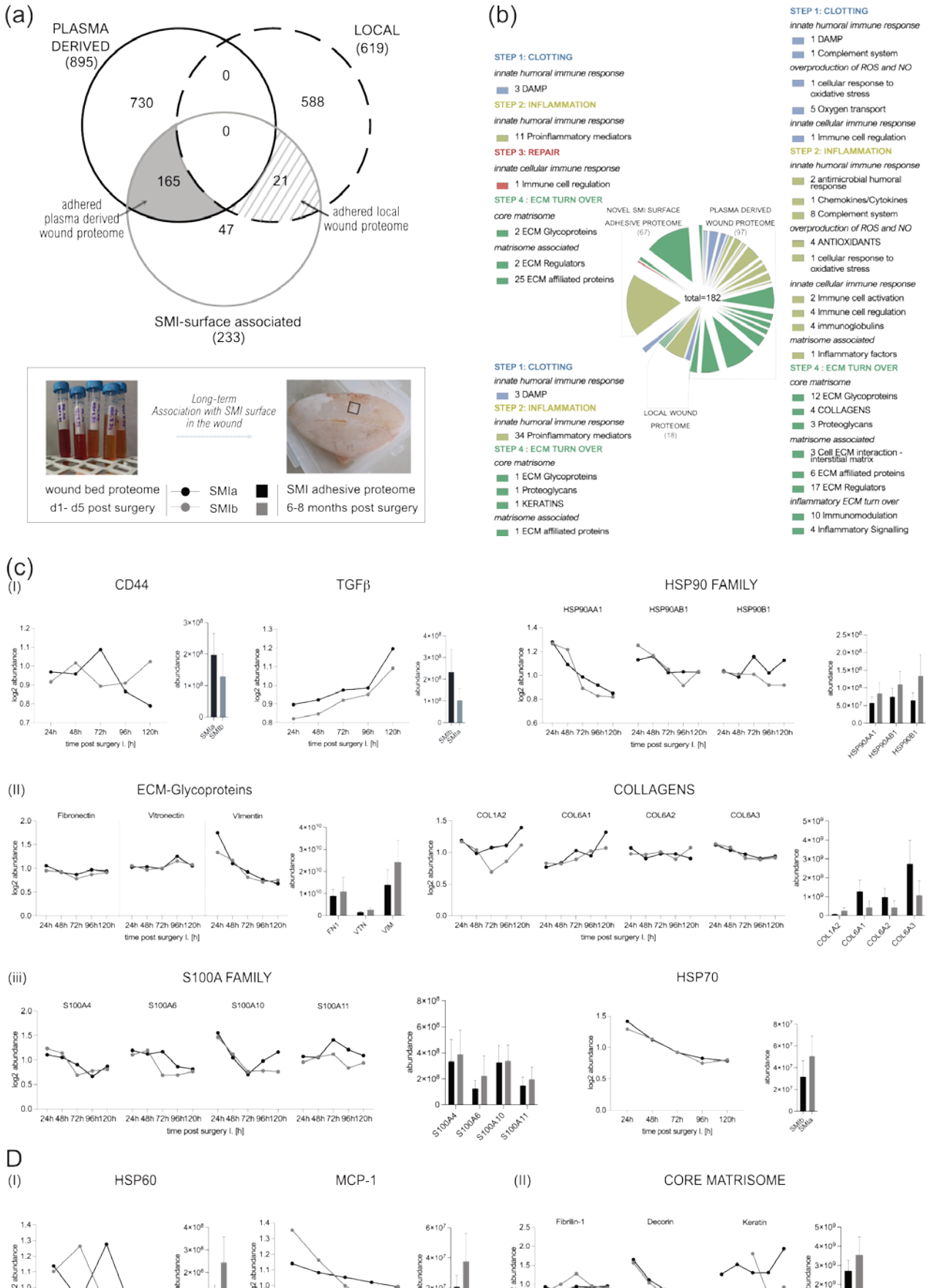

 doi:10.20944/preprints202212.0004.v1

Figure 7. From wound to fibrosis. Comparative analysis of SMI-associated proteome 8 months post-op recruited and adhered from wound proteome 1-5 days post-SMI implantation. **(a)** Venn diagram showing the distribution of plasma-derived and local acute wound proteins associated at silicone tissue expander surface (SMIa: 4μM and SMIb 60μM surface roughness) 6-8 months post-implantation. (b) Functional categorization of SMI-associated wound proteome in the context of wound healing /tissue repair of common and origin. **(c-d)** Comparative analysis of protein abundance in wound bed fluid 1-5 days post-implantation (Left; dots with connecting lines, median shown) and associated on SMI surface 6-8 months post-op (Right; bars, shown mean ±SD,): **(c)** plasma-derived (i) inflammatory response, (ii) ECM turn over and (iii) profibrotic mediation as well as **(d)** local proinflammatory monocyte attraction and (ii) ECM-turn over. The level for statistical significance was set at $p^{ns} \geq 0.05$, p*<0.05, p**<0.002, p***<0.0002, and p****<0.0001, for all statistical tests. (inter- and intra-individual comparison; n=7)

4. Discussion

There is a tendency of autoimunologists to forbid SMIs altogether, due to,e.g. the high percentage of SMI carriers presenting with circulating proteins - antibodies against G protein-coupled receptors (GPCRs) in small autonomic nerve fibers[58].

Intraindividual comparative proteomic profiling in plasma, wound, and SMI-adhesive proteome

Any implanted foreign body elicits an immediate inflammatory response resulting in either fibrous encapsulation by excessive ECM turn-over or incorporation of the implanted biomaterial [59]. The controlled method of sample collection, as well as the analysis used, is an integral step in biological significance in the diagnostic research process of capsular fibrosis etiology.

Blood biomarkers are widely applied for screening and diagnosis of inflammation, because of their availability. However, the extent of the soft tissue reaction surrounding the implant depends on several factors, though to study wound infection directly, wound bed fluid is the prerequisite sample to choose. It is not only tied to the wound bed environment but is easily available. Proteins in wound fluid obtained by sterile, closed suction drain placed in the subcutaneous tissue (following mastectomy)[48], are not only exposed to proteinase 3 [60] but also plasminogen activity [61]. Moreover, drain collection from day 1 to day 5 post-implantation in flasks stored at room temperature, establishes a 24h time window of proteomic degradation.

Identification of protein repertoires in the wound bed fluid directly after SMI implantation is notoriously challenging for the discovery of potential biomarkers for the switch and progression from normal healing response towards chronic fibrosis and excessive encapsulation of the silicon device. Moreover, protein adsorption at the implant surface is a key driver of local reactions to silicone, thus we aimed to identify proteins that surround the device non-specifically in the acute wound and adhere to the silicon surface.

In this study we investigated the proteomes of pre-operative plasma (-1d), - wounds derived from surgical drainages following NSME (d1-d5) and associated with/adhered to the SMI surface app. 8 months post-op.

The etiology of this exaggerated capsule formation has been multifactorial but primarily induced by immune mechanisms toward the foreign material silicone. First time performed *in vivo*, in human patients, we decided to identify, characterize and quantify intra-individually the global FBR against SMI, common to two commercially available tissue expanders with varied surface roughness and topography: the SMIa with reduced surface roughness (4μM Ra; SmoothSilk®, Motiva) and conventional SMIb (60μM Ra; CPX® 4, Mentor). Sample collection was performed simultaneously for both devices in a sterile environment from the same individuum at the same time point (n=7) (Figure 1-2). Here, we provide insight into a set of diagnostic biomarkers applicable to silicone devices with varying surface topography roughness.

Immunomics: The essence lies in sample integrity

 doi:10.20944/preprints202212.0004.v1

Investigation of wound proteome revealed an SMI common, topography independent, as well as topography exclusive wound and adhesive proteome (Figure 3a and Figure 6a). We show a high abundance correlation between the biological and technical replicates of wound fluid and tissue expander surface samples (WBF: Figure 3c, Supplementary Figure S1, and SMI surface-adhesive proteome: Figure 6b and Supplementary Figure S2), validating our intra-individually analyzed dataset. Additionally, there were few differences regarding the total spectral count between groups, validating the sample preparation and allowing for semi-quantitative comparison between plasma and plasma-derived wound proteome.

Corresponding to previous studies [49], we found significantly higher protein numbers in wound bed fluid compared to plasma (Figure 3a). Our analysis demonstrated a high inter-individual sample variance and intra-individual composition, between plasma and acute wound fluids as well as a collection time-point variation within wound samples from NSME drainages collected 1-5 days post-surgery (Figure 3b). Furthermore, the protein substrate environment varied between groups, as the wound fluid samples contained a more varied environment as compared to plasma (Figures 3b).

As neutrophil proteases are acquired in a dose-dependent manner from activated neutrophils during inflammation [62], we hypothesized that the interindividual sample distribution and variation could be influenced by differences in the respective protease environments due to collection time-point. The inter-individual differences seen in the SMI-common wound and adhesive proteomes are most likely due to individual changes in substrate abundance and protease expression [49, 63].

Taken together, these results serve as proof of the principle that intraindividual comparison and analysis of proteomes can indeed withstand detectable inter-individual differences in common protein expression and is crucial for immunoreactivity data comparison of SMI with varied topographies, in a general overview of silicone device immunoreactivity.

Immediate inflammatory rush in the wound after SMI implantation

The characterization and quantification of inflammatory composition and kinetics in wound bed fluid and the verification of adhered wound proteome on the SMI surface proved as a valuable strategy for the possible development of diagnostic tests for subclinical capsular fibrosis.

The common wound bed proteome was composed of a plasma-derived and local wound protein fraction generated around both devices (Figure 3a). Quantification of plasma-derived proteins in wound fluid has shown significantly higher protein expression in wound bed fluid post-op compared to plasma pre-op, which decreases progressively over the first five days after device implantation, to pre-op levels (Figure 3b and 3f, Supplementary Figure S3c). We also analyzed the wound proteome derived from local tissues and demonstrated the same progressive reduction in protein abundance, respectively ((Figure 4e, Supplementary Figure S4c).

First time, in a clinically synchronized controlled setting, intra-individual in humans, with fresh, sterile, time-point-specific collected samples, our results significantly expand the number and origin classification of inflammatory wound bed proteome. In this present investigation, DEPs with high significance in wound fluid and adhered to SMI, such as the HSP90 family, collagens, and S100A family are actively associated with phases of disturbed wound healing (clotting, inflammation, fibrotic repair, and excessive ECM turnover) and can be further characterized as inflammatory matrisome.

Pathogen binding and activation of inflammasome in the wound

Immediately following the placement of a breast implant, the destruction of the tissue initiates the host response to reactive oxygen species (ROS), nitric oxide, and toxic and mechanical stress [11, 29]. The first remarkable result to emerge from the data is 34

 doi:10.20944/preprints202212.0004.v1

plasma-derived DEPs with high significance, such as Superoxide dismutase (Periredoxin, Extracellular and mitochondrial) and Catalase (Supplementary Tables S9) are actively involved in oxidative response to NO and ROS. However, we found no expression of additional ROS or NO disbalance responders in the local wound compartment.

Increased expression of plasma-derived PAL-1 during the first five days after implantation was observed. This factor plays an essential role in blood coagulation, by inhibiting the conversion of plasminogen to plasmin, thereby preventing fibrinolysis [64, 65]. Moreover, we observed elevated levels of plasma-derived HBB, HBA2, MB, HBD, HBG1, and locally expressed in the wound HBG2, which reflects the first response to tissue damage- bleeding and clotting. Damage to epithelial cells leads to the aggregation of erythrocytes and platelets that form a blood clot to contain the spreading of the damage.

The destruction of the tissue and accumulation of altered self-components as well as reactions to noninfectious foreign material triggers inflammation and the release of damage-associated molecular patterns (DAMPs), or allows the entrance of microorganisms and thereby pathogen-associated molecular patterns (PAMPs) [29]. To our surprise, we found PGLYRP1 differentially expressed in the local environment. This 196aa innate immunity protein acts as a bactericidal pattern receptor that binds to murein peptidoglycans (PGN) of Gram-positive bacteria [66]. Moreover, in this present investigation, we could confirm the abundance of LBP, BPI, CFL1, CAMP, LYZ, and B2M in the wound. 15 plasma-derived DEPs with high significance, such as CAMP, LTF, DEFA1B, and ITGB2 are actively associated with host-pathogen interaction and antimicrobicidal response. CAMP, a 177aa cationic antimicrobial protein with a molecular mass of 18kDa, is an acute-phase reactant that binds to bacterial lipopolysaccharides (LPS) [67, 68] and acts via neutrophil N-formyl peptide receptors to enhance the release of CXCL2 [69].

FBR and Inflammation: The response in inflammatory matrisome

Local cells such as dendritic cells and macrophages are activated by DAMPs and PAMPs through toll-like receptors (TLRs) and protease-activated receptors (PARs) and produce the first round of pro-inflammatory mediators [11]. Interestingly the PGRP1, detected in the local wound environment, acts in complex with the Ca2+-binding protein S100A4 as a chemoattractant able to induce lymphocyte movement [70]. The abundance of plasma-derived S100A4, as well as differentially expressed CD44 and MNDA, could be confirmed in the wound environment (Supplementary material, Table S8).

In our study, strong evidence was found in GO enrichment analysis of plasma-derived and local wound proteins, revealing highly significant involvement in biological processes of neutrophil, granulocyte, and leucocyte activation, mediation, and degranulation (Figure 4a), which confirms an infiltration of neutrophils and monocytes that respond to the pro-inflammatory stimuli at the implant surface. Phagocytes such as neutrophils and macrophages remove tissue debris and potentially threatening particles, whereas neutrophil and granulocyte degranulation induce the first inflammatory storm [11, 29].

The granules of neutrophils contain numerous enzymes, such as matrix metalloproteinases (MMPs), elastase, and cathepsins that can specifically cleave collagenous and non-collagenous connective tissue components mandatory for pro-fibrotic ECM turnover. Correspondingly, we identified plasma-derived DEPs involved in ECM remodeling, such as ELANE, Leucocyte elastase inhibitor (SERPINB1), and NCF1B as well as MMP2, MMP8 and MMP9 (Supplementary material, Table S8). Moreover, neutrophils play an indirect role by activating further innate cellular components[30, 62], reflected in highly significant DEPs such as CSF1R, and BCAP31 (Supplementary material, Table S8).

In a pro-inflammatory environment, activated monocytes and resident macrophages(M1) produce pro-inflammatory mediators such as IL-6, TNF-α, and IL-1[71]. We detected IL1RN, IL1RAP in plasma-derived (Supplementary Table S8) and IL1R2, IL6ST in local wound proteome (Supplementary material, Table S14). Our findings confirm the

 doi:10.20944/preprints202212.0004.v1

presence of activated macrophages in the wound environment that produce IL-1 to activate fibroblasts and induce the overproduction of ECM proteins. Although we did not identify TNF-α components in the wound proteome we detected TNF-α-triggered signal transduction via the NF-κB pathway reflected in the local expression of tumor necrosis factor receptor superfamily member 10C and NFKB1 (Supplementary material, Table S14).

Remarkably, traces of antifibrotic effected by interferon (IFN)-γ produced ls were visible in plasma-derived and local interferon-inducible components IFIT3 (Supplementary Table 8), IFIT2, IFI30, IFI35, and IFI16 (Supplementary material, Table S14). Effective healing is usually characterized by a dominant T helper 1 (Th1) cell response, whereas a predominant T helper 2 (Th2) response and an increase in T helper 17 (Th17) cells lead to chronic inflammation, which can ultimately result in fibrosis [29]. Whereas Th2 cells mediate adaptive immune response to injury by producing pro-fibrotic (anti-inflammatory) cytokines (e.g., IL-4, IL-13, IL-10), Th1 cells mediate tissue damage response by Th1-related proinflammatory cytokines (IFN-y, IL-12) that suppress fibroblast- induced collagen synthesis and attenuate fibrosis[72]. In addition, IFN-γ production up-regulates the expression of matrix metalloproteinases (MMPs), whose proteolytic activity helps alter ECM remodeling. As a commonly recognized opponent of Th1 cells, Th2 cells can alter Th1-associated IFN-γ expression levels and high levels of Th2 cytokines have been reported in several fibrotic diseases [73].

Taken together, we have obtained comprehensive results demonstrating two main implant-induced pro-fibrotic progressions- a systemic (plasma-derived) proinflammatory response and local proinflammatory mediation in the wound. The wound bed proteome analysis post silicon implantation provides detailed insights into wound healing stages characterized by various inflammatory matrisome proteins.

From wound to fibrosis

In the course of wound healing, inflammatory responses subside and turn into repair responses through the effects of anti-inflammatory and pro-repair cytokines. In accordance, we found Transforming growth factor-beta-induced protein (TGFB1, Supplementary material, Table S8) as a compound of the plasma-derived protein and locally expressed Late Transforming growth factor binding protein LTBP4, LTBP2 as well as LTBP1 (Supplementary Table S14), the latter being differentially expressed over the first five days after SMI implantation (Figure 5g, Supplementary material, Table S15). LTBPs are involved in fibroblast proliferation and migration; thus, with the finding of plasma-derived SLC9A3R1 and local CRYAB we provide further evidence for the stage of fibrogenesis and fibroblast proliferation into the more contractile myofibroblasts [29]. Myofibroblasts produce an extracellular matrix (ECM) to close the open wound and form a scar[74]. As already reported, active ECM turnover could primarily be suspected through the detection of MMP2, 8, and 9, whereas MMP8 was upregulated in the wound over the total first five days post-surgery. Further, we identified and characterized 71 plasma-derived- and 30 local wound proteins as core matrisome as well as 142 plasma-derived- and 48 local wound proteins as matrisome affiliated proteins [75, 76]. Strikingly, we could identify up-regulated over the first five days post-op not only pro-fibrotic marker COL1A (plasma-derived; Supplementary material, Table S9) and ELANE, but also the fibrosis drivers S100A8 and S100A9 derived from plasma. Also, COL6 and COL3 were detected, however not significantly increased over the total 5-day period (Supplementary material, Table S8). The set of profibrotic markers was supplemented with the locally expressed keratins (Supplementary Table S15: KRT-8, -36, -82, -75, -76 and-79) as well as collagen alpha chains (Supplementary material, Table S15: COL-12A1, -14A1, -15A1 and -18 A1).

Regularly, in the last phase of repair excess, ECM is degraded for incorporation of new cells as the tissue regains its structure and function. However, in fibrosis, aberrant wound healing results in excessive accumulation of collagen and ECM components.

 doi:10.20944/preprints202212.0004.v1

To identify potential biomarkers for the switch and progression from normal healing response towards chronic fibrosis and excessive encapsulation of the silicon device we further focused, not on serum as previously reported [20, 77], but on wound bed fluid proteins, that associated with both silicone surfaces and were still adhered to them after 8 months lingering in the body under pro-inflammatory and pro-fibrotic conditions.

Our data reveals not only a common SMI-associated proteome (Figure 6), independent of surface topography, after 8 months residing in a human body, but also a common implant enclosing wound proteome adhered to SMI surfaces (Figure 7). Enrichment analyses of the common (on SMIa and SMIb) adhesive proteome confirmed the main involvement in ECM turnover reflecting early-stage fibrosis.

Besides the wound-derived proteome, we identified additional 67 proteins, found adhered to SMI surfaces but detected not in wound bed fluid. This early-stage fibrotic set of proteins was characterized by several 60S and 40S ribosomal proteins, a major group of proinflammatory mediators [78–80]. Moreover, we detected CAPG and CD9 on SMI surfaces. This correlates favorably with a recent study in fibrotic adipose tissue, where Rabhi and colleagues [81] have shown that $CD9^{+}$ senescent macrophages activate a fibrotic transcriptional program in adipocyte progenitors.

Strikingly, among the SMI adhesive proteome, we found various collagens and S100A family members (Supplementary Table 17), all previously identified as part of the plasma-derived inflammatory matrisome in the acute wound. In healthy epidermal tissue, collagen type I is more prevalent compared to type III, which makes up about 30% of the total collagen content[82, 83]. Due to ECM turnover during wound healing, COL3 can increase up to 90% and a decrease in type III can lead to excessive scar formation[74]. In contrast with earlier reports, we did not observe a significant upregulation of COL3 but COL1 and COL6 in the acute wound (Supplementary material, Figure S5). However, COL3 was detected on the SMI surface, significantly upregulated on days 3 and 4 post-op and we found higher levels of COL3 compared to COL1 in the acute wound proteome (Table 3). We not only manifest the role of COL1 in late fibrosis [84, 85], our new data may provide information on the chronological production of other collagens and non – collagenous proteins.

Unexpectedly S100A8/A9, a major fibrogenesis marker and fibrosis driver (fibroblast -proliferation, -differentiation, and -activation of collagen production)[86] was found only in the wound environment, whereas S100A4, A6, A10, and A11 associated with the silicon surface (Figure 7 and Supplementary Table 17). The latter was not surprising as S100A4 was identified as a fibrosis driver and as a useful biomarker for diagnosis and monitoring disease progression [70]. Our experiments not only corroborate with previous studies, here we provide discrimination of roles in fibrosis for the S100A family, S100A8/9 marking early inflammatory profibrotic process where S100A4, exerts its pro-inflammatory role in early-stage fibrosis 8 months after SMI implantation. Furthermore, multiple processes involved in fibroblast activation on the SMI surface were reflected by confirmation of HSP90 adhesion to the implant site (Figure 7 and Supplementary material, Table 17). HSPs are involved in the activation or inhibition of epithelial-mesenchymal transition signaling pathways and the generation and degradation of extracellular matrix to regulate fibrotic diseases, thus we were not surprised to find HSPA1B, HSPA8, HSPB1 (plasma-derived; Supplementary material, Table 17) and HSPD1(local; Supplementary material, Table 18) attached to the surface [21].

Moreover, we can demonstrate a chronic fibrotic signaling axis, with PGLYRP1, part of the ant microbicidal response in a wound, that forms an equimolar complex with heat shock protein HSPA1A (on expanders) and activates the TNFR1 receptor (expressed locally TNF superfamily 10) from the immediate inflammatory response to chronic inflammation 6-8 months after SMI implantation.

Strikingly, HSP60 a part of the antimicrobial inflammatory response[87] in the acute wound was found attached to the silicon shell surface. The stress-induced protein is involved in bystander activation of T cells. By inducing secretion of the proinflammatory

 doi:10.20944/preprints202212.0004.v1

cytokine IFN-γ [88] it acts directly on activating bacterial HSP-responsive gamma delta T cells[87]. It can also act as a target for autoreactive hsp60-specific T-cell responses and directly contribute to chronicity at the site of inflammation. Hsp60-responsive T cells are pro-inflammatory cells with increased secretion of IFN-γ [88] and low IL-10 profile. Involved in human chronic inflammatory diseases of Th1 and Th2 cells, it can majorly distract wound healing [89]. Our values correlate favorably well with a series of reports and further support the idea that HSP60, is an essential homeostatic antigen, with both, immunoregulatory and inflammatory properties. Its abundance confirms the presence of antimicrobial antigens and response in the wound after SMI implantation. However, the signaling of an endogenous protein expressed in low amounts chronically attached to SMI surfaces may lead to distinct patterns of activation of TRL-expressing cells such as dendritic cells, macrophages, and T cells, the pathology of fibrosis.

Derived from wound proteome, detection of CCT8 (local) and T_{REG} receptor CD44 (plasma-derived), both adhered to SMI surfaces (Supplementary Table S18), clearly confirm T cell response at and directed to the implant site. Only scarce data about specific local side effects (local immune response, activity of immune cells) focusing on lymphocytes isolated from fibrous capsules were reported so far. In a previous attempt, we characterized the cellular composition of fibrous capsules formed around SMIs, by showing that macrophages and fibroblasts were the most predominant cell populations in the region abutting the silicone surface (designated as “pseudo synovium”) [21]. Strikingly, among T cells, Treg numbers, in peri-SMI fibrotic capsules, were inversely proportional to the degree of fibrosis (Baker scores I to IV). Most interestingly, we showed that Tregs were decreased in those capsules removed from patients with clinically severe symptoms of capsular contracture (Baker scores III to IV) [21].

Thus, we not only deciphered the three-dimensional composition of a silicon implant surface associated/adhesive proteome (Figure 8), by identifying the adhesion of (i) plasma and local tissue-derived proteins in the acute wound and (ii) components expressed later in the early stages of fibrosis. Among these we identified long-term capsular fibrosis markers after a simultaneous NSME and implant-based breast reconstruction, providing novel diagnostic targets for long-term tracking of capsular fibrosis and potential capsular contracture.

Preprints (www.preprints.org) | NOT PEER-REVIEWED | Posted: 1 December 2022 doi:10.20944/preprints202212.0004.v1

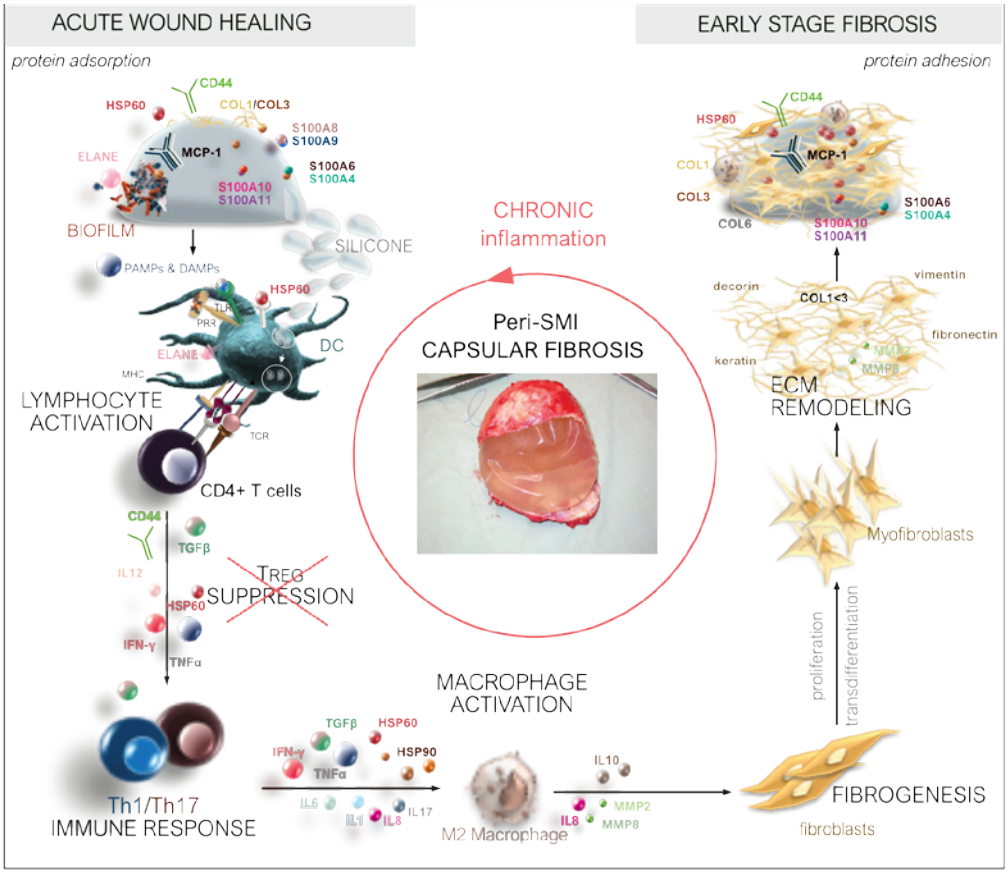

Figure 8. From wound to fibrosis. Chronological orchestration of immediate towards chronic FBR.

As also shown here, the wound and SMI-adhesive proteomes of individuals vary greatly, and therefore investigating specific differences in the groups would benefit from larger sets of data to exclude unreliable findings and intensify the differences. Nevertheless, the fact that significant differences still emerged between the different proteomes, despite the limited patient number, illustrates the power of intraindividual comparison of two different silicone breast implants, in detecting subtle qualitative differences in protein patterns. Moreover, the detection of mammary gland-specific breast cancer marker Mammaglobin A in local wound tissue after bilateral mastectomy in all tested breast cancer patients (no tumor diagnosis yet) strengthens our data integrity immensely and confirms the high specificity but applicability of our approach. Although limited, we demonstrate the power of our combined proteomics and bioinformatics approaches in a detailed immunomic picture of capsular fibrosis etiology- from the immediate inflammatory response to early-stage fibrosis.

Lastly, we would like to highlight our "secondary finding" of the SMI surface topography exclusive acute wound and adhesive proteome. Biomaterial surface chemistry, mechanical properties, and topography have been shown to influence the immune response [17, 34] and implant surface-associated biofilm formation, especially due to antimicrobic (antibiotic)-resistant microbial strains, can lead to chronic immune system activation [90, 91]. However, depending on the topography of these surfaces, varying degrees of capsular contracture are reported [22, 92, 93] and recent studies in rodents and preserved capsular tissue samples have confirmed a reduction of inflammation and foreign body response on implants with an average roughness of 4µm [51]. These results propose a further investigation of surface topography effect on microbiome and proteome composition after breast implant insertion in a controlled clinical setting with breast cancer patients, as demonstrated here.

 doi:10.20944/preprints202212.0004.v1

Our innovative intraindividual comparative molecular identification of biomarkers and their chronological progression, generates information of great importance for a basic understanding of fibrotic side effects of SMIs, in terms of diagnostics prevention, potential new therapeutic approaches as well as improved biocompatibility of SMIs.

5. Conclusions

Our study comprehensively portrayed serum-, wound fluid, and SMI surface adhesion proteomic profiling in patients after simultaneous prophylactic NSME and breast-tissue expander (implant)-based reconstruction. We provide insights into the composition of the wound proteome, comprised of a systemic plasma-derived and a local (expressed in local tissue) wound proteome, the first serving as an inflammatory foreign-body responder, and the second as a proinflammatory mediator. We found massive antimicrobicidal activity and a complex Inflammasome immediately after SMI implantation. This implies microbial colonization and biofilm formation as potential FBR triggers and needs to be investigated in more detail.

First time analyzed in fresh human samples, collected in a controlled clinical setting, these results offer unique evidence for an immediate systemic FBR burst response with a subsequent decline already over the first days as well as proinflammatory mediation from the local tissue in the wound over the first days- and long-term, as adhesive and resident inflammatory matrisome on the SMI surfaces. Our data revealed potential early markers, such as S100A8/A9, and potential long-term markers, including COL1, HSP90, S100A4, and ELANE with high diagnostic sensitivity. Furthermore, the presented results provide preliminary information on DEPs in wound fluid and their possible application for discovering new therapeutic targets to halt the development of capsular contracture and for the identification of further candidate biomarkers of this disease. Therefore, this study and our analytical approach warrant further investigations to comprehensively and conclusively elucidate the role of these proteins in the pathogenesis of capsular fibrosis in implant-based breast reconstruction.

Supplementary Materials: The following supporting information can be downloaded at: www.mdpi.com/xxx/supplementarytables, Table S1: GO enrichment plasma derived wound proteome; Table S2: KEGG enrichment plasma derived wound proteome; Table S3: STRING kmeans(k=4) cluster description of plasma derived wound proteome; Table S4: PPI cluster 4 description of plasma derived wound proteome; Table S5: PPI cluster 2 description of plasma derived wound proteome; Table S6: PPI cluster 1 description of plasma derived wound proteome; Table S7: PPI cluster 3 description of plasma derived wound proteome; Table S8: plasma derived inflammatory matrisome in the acute wound; Table S9: plasma derived inflammatory matrisome DEPs in the acute wound; Table S10: KEGG enrichment PPI cluster 1 description of plasma derived wound proteome; Table S11: KEGG enrichment PPI cluster 3 description of plasma derived wound proteome; Table S12: KEGG enrichment PPI cluster 4 description of plasma derived wound proteome; Table S13: KEGG enrichment PPI cluster 2 description of plasma derived wound proteome; Table S14: local inflammatory matrisome in the acute wound; Table S15: local inflammatory matrisome DEPs in the acute wound; Table S16: SMI surface-associated inflammatory matrisome; Table S17: Plasma derived wound proteome adhesion on SMI-surface; Table S18: Local wound proteome adhesion on SMI-surface; Table S19: chronic wound adhesion on SMI surface.

The following supporting information can be downloaded at: www.mdpi.com/xxx/supplementaryfigures, Figure S1: LC-MS/MS reproducibility and distribution of wound proteins identified in (a) plasma and wound bed fluid formed around (b) SMIa and (c)SMIb; Figure S2: LC-MS/MS reproducibility and distribution of SMI adhesive proteins identified; Figure S3: Intraindividual comparative analysis of plasma-derived DEPs in the acute wound 1-5 days post-SMI implantation; Figure S4: Intraindividual comparative analysis of local DEPs in the acute wound 1-5 days post-SMI implantation; Figure S5. Comparative analysis of collagen abundance in plasma pre-op and wound bed fluid 1-5 days post-implantation.

 doi:10.20944/preprints202212.0004.v1

Author Contributions: D.W. and I.S. conceived the project and designed the experiments. D.E. performed the NSME and D.W. performed tissue-expander-based breast reconstruction. Senior surgeons D.W. and I.S. performed all sample collection experiments together. I.S. prepared the samples for mass spectrometry analysis. K.F. processed all samples and performed all mass spectrometry experiments. I.S. analyzed the data and is responsible for data curation. I.S. wrote the manuscript and performed original draft preparation. D.W., B.S., and K.F. reviewed and edited the original manuscript draft. I.S. visualized all data. K.F. visualized sample preparation for mass spectrometry. I.S. was responsible for project administration. D.W. acquired funding for the project, supervised the clinical trial, and was responsible for the acquisition of the participants´ informed consent.

Funding: Research on this project was funded by Establishment Labs, Costa Rica (ID D152500-015-015) to D.W.

Institutional Review Board Statement: The study was conducted in accordance with the Declaration of Helsinki, and approved by the Institutional Ethics Committee of the Medical University of Innsbruck (protocol code 1325/2019, approved on 23rd January 2020) and the Austrian Federal Office for Safety in Health Care (approval number; 13340962).

Informed Consent Statement: Informed consent was obtained from all subjects involved in the study.

Data Availability Statement: The mass spectrometry proteomics data have been deposited to the ProteomeXchange Consortium (http://proteomecentral.proteomexchange.org) via the iProX partner repository with the dataset identifier PXD00000 and are publicly available as of the date of publication. The data presented in this study are available on request from the corresponding author due to data privacy protection. The trial basic summary results have been deposited within ClinicalTrials.gov (ID) registry and are publicly available as of the date of publication.

Acknowledgments: We thank Christian Ploner (Department for Plastic Surgery, Medical University of Innsbruck) for providing laboratory capacities as well as technical help; Angela Augustin, Selina Winkelman, and Monika Lanthaler for assistance during surgeries and monitoring of appropriate collection of wound bed fluid; Andreas Kuen for mass spectrometrical analysis assistance and Simon Senfter for proteomic sample preparation; Karin Langert and Angelika Feichter for photo documentation of all patients; and Georg Wick (Emeriti; Medical University of Innsbruck) for critical reading and suggestions on the manuscript.

Conflicts of Interest: The authors declare no conflict of interest. The funders had no role in the design of the study; in the collection, analyses, or interpretation of data; in the writing of the manuscript; or in the decision to publish the results.

Appendix A

The following information can be downloaded as an additional file at: www.mdpi.com/xxx/tables, Table 1: Inclusion and exclusion criteria for the Expander-Immunology trial (clinicaltrial.gov ID); Table 2: Intraindividual statistical comparison of analytical groups.; Table 3: Total wound proteome; Table 4: common plasma-derived wound proteome; Table 5: STRING kmeans (k=4) cluster description of plasma-derived wound proteome; Table 6: Numbers of inflammatory matrisome proteins in plasma-derived wound proteome after silicon device implantation.; Table 7: common local wound proteome; Table 8: STRING kmeans cluster description local wound proteome.; Table 9: Numbers of inflammatory matrisome proteins in local wound proteome after silicon device implantation.; Table 10: Total SMI surface-adsorbed proteome Table 11: Common SMI surface-adsorbed proteome; Table 12: Acute wound proteome association with SMI surfaces 6-8 months post-implantation.

References

1. Wynn, TA. 2008. Cellular and molecular mechanisms of fibrosis. *The Journal of Pathology* 214. John Wiley & Sons, Ltd: 199–210. https://doi.org/10.1002/path.2277.
2. Ji, Litong, Tie Wang, Lining Tian, Hongjiang Song, and Meizhuo Gao. 2020. Roxatidine inhibits fibrosis by inhibiting NF-κB and MAPK signaling in macrophages sensing breast implant surface materials. *Molecular Medicine Reports* 21. Spandidos Publications: 161–172. https://doi.org/10.3892/mmr.2019.10815.

3. Kuehlmann, Britta A., Clark Andrew Bonham, and Geoffrey C. Gurtner. 2019. Abstract 114. Targeting Wnt Signaling to Reduce Capsular Fibrosis. *Plastic and Reconstructive Surgery - Global Open* 7. Ovid Technologies (Wolters Kluwer Health): 80. https://doi.org/10.1097/01.gox.0000558388.69103.8d.
4. Kuo, Yao Lung, I. Ming Jou, Seng Feng Jeng, Chun Hui Chu, Jhy Shrian Huang, Tai I. Hsu, Li Ren Chang, Po Wei Huang, Jian An Chen, and Ting Mao Chou. 2019. Hypoxia-induced epithelial-mesenchymal transition and fibrosis for the development of breast capsular contracture. *Scientific Reports* 9. Nature Publishing Group: 1–6. https://doi.org/10.1038/s41598-019-46439-7.
5. Biernacka, Anna, Marcin Dobaczewski, and Nikolaos G. Frangogiannis. 2011. TGF-β signaling in fibrosis. *Growth Factors* 29: 196–202. https://doi.org/10.3109/08977194.2011.595714.
6. Chaikuad, Apirat, and Alex N. Bullock. 2016. Structural basis of intracellular TGF-β signaling: Receptors and smads. *Cold Spring Harbor Perspectives in Biology* 8. Cold Spring Harbor Laboratory Press. https://doi.org/10.1101/cshperspect.a022111.
7. Meng, Xiao Ming, David J. Nikolic-Paterson, and Hui Yao Lan. 2016. TGF-β: The master regulator of fibrosis. *Nature Reviews Nephrology*. Nature Publishing Group. https://doi.org/10.1038/nrneph.2016.48.
8. Lan, Hui Yao. 2011. Diverse roles of TGF-β/Smads in renal fibrosis and inflammation. *International Journal of Biological Sciences*. Ivyspring International Publisher. https://doi.org/10.7150/ijbs.7.1056.
9. Margadant, Coert, and Arnoud Sonnenberg. 2010. Integrin-TGF-B crosstalk in fibrosis, cancer and wound healing. *EMBO Reports*. https://doi.org/10.1038/embor.2009.276.
10. Hu, He He, Dan Qian Chen, Yan Ni Wang, Ya Long Feng, Gang Cao, Nosratola D. Vaziri, and Ying Yong Zhao. 2018. New insights into TGF-β/Smad signaling in tissue fibrosis. *Chemico-Biological Interactions*. Elsevier Ireland Ltd. https://doi.org/10.1016/j.cbi.2018.07.008.
11. Wick, Georg, Cecilia Grundtman, Christina Mayerl, Thomas-Florian Florian Wimpissinger, Johann Feichtinger, Bettina Zelger, Roswitha Sgonc, and Dolores Wolfram. 2013. *The immunology of fibrosis*. *Annual Review of Immunology*. Vol. 31. https://doi.org/10.1146/annurev-immunol-032712-095937.
12. Wynn, Thomas A. 2007. Common and unique mechanisms regulate fibrosis in various fibroproliferative diseases. *The Journal of clinical investigation* 117. J Clin Invest: 524–529. https://doi.org/10.1172/JCI31487.
13. Siggelkow, Wulf, Andre Faridi, Katrin Spiritus, Uwe Klinge, Werner Rath, and Bernd Klosterhalfen. 2003. Histological analysis of silicone breast implant capsules and correlation with capsular contracture. *Biomaterials* 24. Elsevier: 1101–1109. https://doi.org/10.1016/S0142-9612(02)00429-5.
14. Handel, N., J. A. Jensen, Q. Black, J. R. Waisman, and M. J. Silverstein. 1995. The fate of breast implants: A critical analysis of complications and outcomes. *Plastic and Reconstructive Surgery* 96. Lippincott Williams and Wilkins: 1521–1533. https://doi.org/10.1097/00006534-199512000-00003.
15. Siggelkow, Wulf, D. M. Gescher, A. Siggelkow, D. Klee, E. Malik, W. Rath, and A. Faridi. 2004. In vitro analysis of modified surfaces of silicone breast implants. *International Journal of Artificial Organs* 27. Wichtig Editore s.r.l.: 1100–1108. https://doi.org/10.1177/039139880402701214.
16. Prantl, Lukas, Stephan Schreml, Stefan Fichtner-Feigl, Nina Pöppl, Marita Eisenmann-Klein, Hartmut Schwarze, and Bernd Füchtmeier. 2007. Clinical and morphological conditions in capsular contracture formed around silicone breast implants. *Plastic and reconstructive surgery* 120. Plast Reconstr Surg: 275–284. https://doi.org/10.1097/01.PRS.0000264398.85652.9A.
17. Mempin, Maria, Honghua Hu, Durdana Chowdhury, Anand Deva, and Karen Vickery. 2018. The A, B and C's of silicone breast implants: Anaplastic large cell lymphoma, biofilm and capsular contracture. *Materials*. MDPI AG. https://doi.org/10.3390/ma11122393.
18. Bizjak, Mojca, Carlo Selmi, Sonja Praprotnik, Or Bruck, Carlo Perricone, Michael Ehrenfeld, and Yehuda Shoenfeld. 2015. Silicone implants and lymphoma: The role of inflammation. *Journal of Autoimmunity*. Academic Press. https://doi.org/10.1016/j.jaut.2015.08.009.
19. Wolfram, D., B. Oberreiter, C. Mayerl, E. Soelder, H. Ulmer, H. Piza-Katzer, G. Wick, and A. Backovic. 2008. Altered systemic serologic parameters in patients with silicone mammary implants. *Immunology Letters* 118. Immunol Lett: 96–100. https://doi.org/10.1016/j.imlet.2008.03.007.
20. Backovic, Aleksandar, Dolores Wolfram, Barbara Del-Frari, Hildegunde Piza, Lukas A. Huber, and Georg Wick. 2007. Simultaneous analysis of multiple serum proteins adhering to the surface of medical grade polydimethylsiloxane elastomers. *Journal of Immunological Methods* 328: 118–127. https://doi.org/10.1016/j.jim.2007.08.016.
21. Wolfram, Dolores, Christian Rainer, Harald Niederegger, Hildegunde Piza, and Georg Wick. 2004. Cellular and molecular composition of fibrous capsules formed around silicone breast implants with special focus on local immune reactions *. *Journal of Autoimmunity* 23. Academic Press: 81–91. https://doi.org/10.1016/j.jaut.2004.03.005.
22. Cappellano, Giuseppe, Christian Ploner, Susanne Lobenwein, Sieghart Sopper, Paul Hoertnagl, Christina Mayerl, Nikolaus Wick, Gerhard Pierer, Georg Wick, and Dolores Wolfram. 2018. Immunophenotypic characterization of human T cells after in vitro exposure to different silicone breast implant surfaces. *PLoS ONE*. https://doi.org/10.1371/journal.pone.0192108.
23. Wolfram, Dolores, Evelyn Rabensteiner, Cecilia Grundtman, Günther Böck, Christina Mayerl, Walther Parson, Giovanni Almanzar, Carlo Hasenöhrl, Hildegunde Piza-Katzer, and Georg Wick. 2012. T regulatory cells and TH17 cells in peri-silicone implant capsular fibrosis. *Plastic and Reconstructive Surgery*. https://doi.org/10.1097/PRS.0b013e31823aeacf.
24. Borkner, Christian B., Stefanie Wohlrab, Eva Möller, Gregor Lang, and Thomas Scheibel. 2017. Surface Modification of Polymeric Biomaterials Using Recombinant Spider Silk Proteins. *ACS Biomaterials Science and Engineering* 3. American Chemical Society: 767–775. https://doi.org/10.1021/acsbiomaterials.6b00306.

25. Witherel, Claire E., Daniel Abebayehu, Thomas H. Barker, and Kara L. Spiller. 2019. Macrophage and Fibroblast Interactions in Biomaterial-Mediated Fibrosis. *Advanced Healthcare Materials* 8. Wiley-VCH Verlag: 1801451. https://doi.org/10.1002/adhm.201801451.
26. Kang, Sunah, Jungah Kim, Seulah Kim, Maierdanjiang Wufuer, Sohyun Park, Yumin Youngmin Kim, Dongkil Choi, et al. 2020. Efficient reduction of fibrous capsule formation around silicone breast implants densely grafted with 2-methacryloyloxyethyl phosphorylcholine (MPC) polymers by heat-induced polymerization. *Biomaterials Science* 8. Royal Society of Chemistry: 1580–1591. https://doi.org/10.1039/c9bm01802f.
27. Swartzlander, Mark D., Christopher A. Barnes, Anna K. Blakney, Joel L. Kaar, Themis R. Kyriakides, and Stephanie J. Bryant. 2015. Linking the foreign body response and protein adsorption to PEG-based hydrogels using proteomics. *Biomaterials* 41. Elsevier Ltd: 26–36. https://doi.org/10.1016/j.biomaterials.2014.11.026.
28. Zeplin, P H, A-K Berninger, N C Maksimovikj, P van Gelder, T Scheibel, and H Walles. 2014. [Improving the biocompatibility of silicone implants using spider silk coatings: immunohistochemical analysis of capsule formation]. *Handchirurgie, Mikrochirurgie, plastische Chirurgie : Organ der Deutschsprachigen Arbeitsgemeinschaft fur Handchirurgie : Organ der Deutschsprachigen Arbeitsgemeinschaft fur Mikrochirurgie der Peripheren Nerven und Gefasse : Organ der V...* 46. https://doi.org/10.1055/s-0034-1395558.
29. Wick, Georg, Aleksandar Backovic, Evelyn Rabensteiner, Nadine Plank, Christian Schwentner, and Roswitha Sgonc. 2010. The immunology of fibrosis: innate and adaptive responses. *Trends in Immunology*. https://doi.org/10.1016/j.it.2009.12.001.
30. Lefkowitz, Doris L., and Stanley S. Lefkowitz. 2001. Macrophage-neutrophil interaction: A paradigm for chronic inflammation revisited. *Immunology and Cell Biology* 79. Immunol Cell Biol: 502–506. https://doi.org/10.1046/j.1440-1711.2001.01020.x.
31. Duffield, Jeremy S., and Mark L. Lupher. 2010. PRM-151 (recombinant human serum amyloid P/pentraxin 2) for the treatment of fibrosis. *Drug News and Perspectives*. https://doi.org/10.1358/dnp.2010.23.5.1444206.
32. Sugimoto, Michelle A., Juliana P. Vago, Mauro Perretti, and Mauro M. Teixeira. 2019. Mediators of the Resolution of the Inflammatory Response. *Trends in Immunology*. Elsevier Ltd. https://doi.org/10.1016/j.it.2019.01.007.
33. Wynn, Thomas A. 2007. Common and unique mechanisms regulate fibrosis in various fibroproliferative diseases. *Journal of Clinical Investigation*. https://doi.org/10.1172/JCI31487.
34. Zhang, Mengjuan, and Song Zhang. 2020. T Cells in Fibrosis and Fibrotic Diseases. *Frontiers in Immunology*. Frontiers Media S.A. https://doi.org/10.3389/fimmu.2020.01142.
35. Pellicoro, Antonella, Prakash Ramachandran, John P. Iredale, and Jonathan A. Fallowfield. 2014. Liver fibrosis and repair: Immune regulation of wound healing in a solid organ. *Nature Reviews Immunology*. Nature Publishing Group. https://doi.org/10.1038/nri3623.
36. Sindrilaru, Anca, and Karin Scharffetter-Kochanek. 2013. Disclosure of the Culprits: Macrophages—Versatile Regulators of Wound Healing. *Advances in Wound Care* 2. Mary Ann Liebert Inc: 357–368. https://doi.org/10.1089/wound.2012.0407.
37. Implants, Institute of Medicine (US) Committee on the Safety of Silicone Breast, Stuart Bondurant, Virginia Ernster, and Roger Herdman. 1999. Immunology of Silicone. National Academies Press (US).
38. Greisler, Howard P. 1990. Interactions at the blood/material interface. *Annals of vascular surgery* 4. Ann Vasc Surg: 98–103. https://doi.org/10.1007/BF02042699.
39. Faruq, Omar, Pham Ngoc Chien, Nilsu Dönmez, Sun Young Nam, and Chan Yeong Heo. 2021. Functionalization of Silicone Surface with Drugs and Polymers for Regulation of Capsular Contracture. *Polymers* 13. Multidisciplinary Digital Publishing Institute (MDPI). https://doi.org/10.3390/POLYM13162731.
40. Naidu, S. H., P. Beredjiklian, L. Adler, F. W. Bora, and D. G. Baker. 1996. In vivo inflammatory response to silicone elastomer particulate debris. *The Journal of hand surgery* 21. J Hand Surg Am: 496–500. https://doi.org/10.1016/S0363-5023(96)80369-8.
41. Hallab, Nadim James, Lauryn Samelko, and Dennis Hammond. 2019. The Inflammatory Effects of Breast Implant Particulate Shedding: Comparison With Orthopedic Implants. *Aesthetic Surgery Journal* 39. Oxford University Press: S36. https://doi.org/10.1093/ASJ/SJY335.
42. Atiyeh, Bishara, and Saif Emsieh. 2022. Effects of Silicone Breast Implants on Human Cell Types In Vitro: A Closer Look on Host and Implant. *Aesthetic Plastic Surgery* 46. Springer: 2609–2611. https://doi.org/10.1007/s00266-022-02821-x.
43. Xing, S., J. P. Santerre, R. S. Labow, and E. L. Boynton. 2002. The effect of polyethylene particle phagocytosis on the viability of mature human macrophages. *Journal of Biomedical Materials Research* 61: 619–627. https://doi.org/10.1002/jbm.10078.
44. Tavazzani, F., S. Xing, J. E. Waddell, D. Smith, and E. L. Boynton. 2005. In vitro interaction between silicone gel and human monocyte-macrophages. *Journal of biomedical materials research. Part A* 72. J Biomed Mater Res A: 161–167. https://doi.org/10.1002/JBM.A.30181.
45. Barr, Simon Patrick, Ernie W Hill, and Ardeshir Bayat. 2018. Novel Proteomic Assay of Breast Implants Reveals Proteins With Significant Binding Differences: Implications for Surface Coating and Biocompatibility. *Aesthetic Surgery Journal* 38. Oxford University Press: 962–969. https://doi.org/10.1093/asj/sjy018.
46. Backovic, Aleksandar, Hong Lei Huang, Barbara del Frari, Hildegunde Piza, Lukas A. Huber, and Georg Wick. 2007. Identification and dynamics of proteins adhering to the surface of medical silicones in vivo and in vitro. *Journal of Proteome Research* 6. J Proteome Res: 376–381. https://doi.org/10.1021/pr0603755.
47. Staiano-Coico, L., P. J. Higgins, S. B. Schwartz, A. J. Zimm, and J. Goncalves. 2000. Wound fluids: a reflection of the state of healing. *Ostomy/wound Management* 46: 85S-93S; quiz 94S.

48. Harvey, Joe, Kieran T. Mellody, Nicky Cullum, Rachel E.B. Watson, and Jo Dumville. 2022. Wound fluid sampling methods for proteomic studies: A scoping review. *Wound Repair and Regeneration* 30. John Wiley and Sons Inc: 317–333. https://doi.org/10.1111/WRR.13009.
49. Hartman, Erik, Karl Wallblom, Mariena J.A. van der Plas, Jitka Petrlova, Jun Cai, Karim Saleh, Sven Kjellström, and Artur Schmidtchen. 2021. Bioinformatic Analysis of the Wound Peptidome Reveals Potential Biomarkers and Antimicrobial Peptides. *Frontiers in Immunology* 11. Frontiers Media S.A.: 3765. https://doi.org/10.3389/FIMMU.2020.620707/BIBTEX.
50. Kappel, Rita M, Antonius J H Klunder, and Ger J M Pruijn. 2022. Silicon chemistry and silicone breast implants. https://doi.org/10.1007/s00238-013-0914-4.
51. Doloff, Joshua C., Omid Veiseh, Roberto de Mezerville, Marcos Sforza, Tracy Ann Perry, Jennifer Haupt, Morgan Jamiel, et al. 2021. The surface topography of silicone breast implants mediates the foreign body response in mice, rabbits and humans. *Nature Biomedical Engineering 2021 5:10* 5. Nature Publishing Group: 1115–1130. https://doi.org/10.1038/s41551-021-00739-4.
52. Shahinuzzaman, A. D.A., Jayanta K. Chakrabarty, Zixiang Fang, David Smith, Abu Hena Mostafa Kamal, and Saiful M. Chowdhury. 2020. Improved in-solution trypsin digestion method for methanol–chloroform precipitated cellular proteomics sample. *Journal of Separation Science* 43. Wiley-VCH Verlag: 2125–2132. https://doi.org/10.1002/JSSC.201901273.
53. Heberle, Henry, Vaz G. Meirelles, Felipe R. da Silva, Guilherme P. Telles, and Rosane Minghim. 2015. InteractiVenn: A web-based tool for the analysis of sets through Venn diagrams. *BMC Bioinformatics* 16. BioMed Central Ltd.: 1–7. https://doi.org/10.1186/S12859-015-0611-3/FIGURES/4.
54. Metsalu, Tauno, and Jaak Vilo. 2015. ClustVis: a web tool for visualizing clustering of multivariate data using Principal Component Analysis and heatmap. *Nucleic Acids Research* 43. Oxford Academic: W566–W570. https://doi.org/10.1093/NAR/GKV468.
55. Ge, Steven Xijin, Dongmin Jung, Dongmin Jung, and Runan Yao. 2020. ShinyGO: a graphical gene-set enrichment tool for animals and plants. *Bioinformatics* 36. Oxford Academic: 2628–2629. https://doi.org/10.1093/BIOINFORMATICS/BTZ931.
56. Goedhart, Joachim, and Martijn S. Luijsterburg. 2020. VolcaNoseR is a web app for creating, exploring, labeling and sharing volcano plots. *Scientific Reports 2020 10:1* 10. Nature Publishing Group: 1–5. https://doi.org/10.1038/s41598-020-76603-3.
57. D480-D489. 2021. UniProt: the universal protein knowledgebase in 2021 The UniProt Consortium. *Nucleic Acids Research* 49. https://doi.org/10.1093/nar/gkaa1100.
58. Halpert, Gilad, Abdulla Watad, Avishai M. Tsur, Arad Dotan, Hector Enrique Quiros-Lim, Harald Heidecke, Boris Gilburd, et al. 2021. Autoimmune dysautonomia in women with silicone breast implants. *Journal of Autoimmunity* 120. Academic Press: 102631. https://doi.org/10.1016/J.JAUT.2021.102631.
59. Anderson, James M. 2008. Biocompatibility and Bioresponse to Biomaterials. *Principles of Regenerative Medicine*. Academic Press: 704–723. https://doi.org/10.1016/B978-012369410-2.50042-5.
60. He, Y., P. K. Young, and F. Grinnell. 1998. Identification of Proteinase 3 as the Major Caseinolytic Activity in Acute Human Wound Fluid. *Journal of Investigative Dermatology* 110. Elsevier: 67–71. https://doi.org/10.1046/J.1523-1747.1998.00075.X.
61. Hoffman, Richard, Sue Starkey, and Jane Coad. 1998. Wound fluid from venous leg ulcers degrades plasminogen and reduces plasmin generation by keratinocytes. *The Journal of investigative dermatology* 111. J Invest Dermatol: 1140–1144. https://doi.org/10.1046/J.1523-1747.1998.00429.X.
62. Jerke, Uwe, Daniel Perez Hernandez, Patrick Beaudette, Brice Korkmaz, Gunnar Dittmar, and Ralph Kettritz. 2015. Neutrophil serine proteases exert proteolytic activity on endothelial cells. *Kidney International* 88. Elsevier: 764–775. https://doi.org/10.1038/KI.2015.159.
63. Schrader, Michael. 2018. Origins, Technological Development, and Applications of Peptidomics. *Methods in molecular biology (Clifton, N.J.)* 1719. Methods Mol Biol: 3–39. https://doi.org/10.1007/978-1-4939-7537-2_1.
64. Ghosh, Asish K., and Douglas E. Vaughan. 2012. PAI-1 in Tissue Fibrosis. *Journal of cellular physiology* 227. NIH Public Access: 493. https://doi.org/10.1002/JCP.22783.
65. Reilly, C. F., and J. E. Hutzelmann. 1992. Plasminogen activator inhibitor-1 binds to fibrin and inhibits tissue-type plasminogen activator-mediated fibrin dissolution. *Journal of Biological Chemistry* 267. Elsevier: 17128–17135. https://doi.org/10.1016/S0021-9258(18)41903-5.
66. Kang, Daiwu, Gang Liu, Annika Lundström, Eva Gelius, and Håkan Steiner. 1998. A peptidoglycan recognition protein in innate immunity conserved from insects to humans. *Proceedings of the National Academy of Sciences of the United States of America* 95. Proc Natl Acad Sci U S A: 10078–10082. https://doi.org/10.1073/PNAS.95.17.10078.
67. Li, Xia, Yifeng Li, Huiyun Han, Donald W. Miller, and Guangshun Wang. 2006. Solution structures of human LL-37 fragments and NMR-based identification of a minimal membrane-targeting antimicrobial and anticancer region. *Journal of the American Chemical Society* 128. J Am Chem Soc: 5776–5785. https://doi.org/10.1021/JA0584875.
68. Wang, Guangshun. 2008. Structures of human host defense cathelicidin LL-37 and its smallest antimicrobial peptide KR-12 in lipid micelles. *Journal of Biological Chemistry* 283: 32637–32643. https://doi.org/10.1074/JBC.M805533200.
69. Woloszynek, Josh C., Ying Hu, and Christine T.N. Pham. 2012. Cathepsin G-regulated release of formyl peptide receptor agonists modulate neutrophil effector functions. *The Journal of biological chemistry* 287. J Biol Chem: 34101–34109. https://doi.org/10.1074/JBC.M112.394452.
70. Li, Zhenzhen, Yanan Li, Shuangqing Liu, and Zhihai Qin. 2020. Extracellular S100A4 as a key player in fibrotic diseases. *Journal of Cellular and Molecular Medicine* 24. Wiley-Blackwell: 5973. https://doi.org/10.1111/JCMM.15259.

71. Sheikh, Zeeshan, Patricia J. Brooks, Oriyah Barzilay, Noah Fine, and Michael Glogauer. 2015. Macrophages, foreign body giant cells and their response to implantable biomaterials. *Materials* 8. MDPI AG: 5671–5701. https://doi.org/10.3390/MA8095269.
72. Immunology, TA Wynn - Nature Reviews, and undefined 2004. Fibrotic disease and the TH 1/TH 2 paradigm. *nature.com*.
73. Wynn, Thomas A. 2004. Fibrotic disease and the TH1/TH2 paradigm. *Nature Reviews Immunology*. Nature Publishing Group. https://doi.org/10.1038/nri1412.
74. Volk, Susan W., Yanjian Wang, Elizabeth A. Mauldin, Kenneth W. Liechty, and Sherrill L. Adams. 2011. Diminished Type III Collagen Promotes Myofibroblast Differentiation and Increases Scar Deposition in Cutaneous Wound Healing. *Cells, Tissues, Organs* 194. Karger Publishers: 25. https://doi.org/10.1159/000322399.
75. Tian, Yaqiong, Hui Li, Yujuan Gao, Chuanmei Liu, Ting Qiu, Hongyan Wu, Mengshu Cao, et al. 2019. Quantitative proteomic characterization of lung tissue in idiopathic pulmonary fibrosis. *Clinical Proteomics* 16. BioMed Central: 1–11. https://doi.org/10.1186/S12014-019-9226-4.
76. Bülow, Roman David, and Peter Boor. 2019. Extracellular Matrix in Kidney Fibrosis: More Than Just a Scaffold. *Journal of Histochemistry and Cytochemistry* 67. Histochemical Society: 643. https://doi.org/10.1369/0022155419849388.
77. Araújo-Gomes, Nuno, Francisco Romero-Gavilán, Ana M. Sánchez-Pérez, Marilo Gurruchaga, Mikel Azkargorta, Felix Elortza, María Martinez-Ibañez, Ibon Iloro, Julio Suay, and Isabel Goñi. 2018. Characterization of serum proteins attached to distinct sol–gel hybrid surfaces. *Journal of Biomedical Materials Research - Part B Applied Biomaterials* 106. https://doi.org/10.1002/jbm.b.33954.
78. Suto, Takahito, and Thomas Karonitsch. 2020. The immunobiology of mTOR in autoimmunity. *Journal of Autoimmunity* 110. Academic Press: 102373. https://doi.org/10.1016/J.JAUT.2019.102373.
79. Moon, Yuseok. 2014. Ribosomal Alteration-Derived Signals for Cytokine Induction in Mucosal and Systemic Inflammation: Noncanonical Pathways by Ribosomal Inactivation. *Mediators of Inflammation* 2014. Hindawi Limited. https://doi.org/10.1155/2014/708193.
80. Hadjicharalambous, Marina R., and Mark A. Lindsay. 2020. Idiopathic Pulmonary Fibrosis: Pathogenesis and the Emerging Role of Long Non-Coding RNAs. *International Journal of Molecular Sciences 2020, Vol. 21, Page 524* 21. Multidisciplinary Digital Publishing Institute: 524. https://doi.org/10.3390/IJMS21020524.
81. Rabhi, Nabil, Kathleen Desevin, Anna C. Belkina, Andrew Tilston-Lunel, Xaralabos Varelas, Matthew D. Layne, and Stephen R. Farmer. 2022. Obesity-induced senescent macrophages activate a fibrotic transcriptional program in adipocyte progenitors. *Life Science Alliance* 5. Life Science Alliance LLC. https://doi.org/10.26508/LSA.202101286.
82. Akilbekova, Dana, and Kaitlin M. Bratlie. 2015. Quantitative Characterization of Collagen in the Fibrotic Capsule Surrounding Implanted Polymeric Microparticles through Second Harmonic Generation Imaging. *PLoS ONE* 10. PLOS. https://doi.org/10.1371/JOURNAL.PONE.0130386.
83. Cheung, David T., Paul D. Benya, Natasha Perelman, Paul E. Dicesare, and Marcel E. Nimni. 1990. A highly specific and quantitative method for determining type III/I collagen ratios in tissues. *Matrix (Stuttgart, Germany)* 10. Matrix: 164–171. https://doi.org/10.1016/S0934-8832(11)80165-4.
84. Kuehlmann, Britta, Isabel Zucal, Clark Andrew Bonham, Lydia Marie Joubert, and Lukas Prantl. 2021. SEM and TEM for identification of capsular fibrosis and cellular behavior around breast implants – a descriptive analysis. *BMC Molecular and Cell Biology* 22. BioMed Central. https://doi.org/10.1186/S12860-021-00364-8.
85. Chen, Wei, Jonathan B. Rock, Martha M. Yearsley, Linda D. Ferrell, and Wendy L. Frankel. 2014. Different collagen types show distinct rates of increase from early to late stages of hepatitis C-related liver fibrosis. *Human pathology* 45. Hum Pathol: 160–165. https://doi.org/10.1016/J.HUMPATH.2013.08.015.
86. Araki, Kota, Rie Kinoshita, Nahoko Tomonobu, Yuma Gohara, Shuta Tomida, Yuta Takahashi, Satoru Senoo, et al. 2021. The heterodimer S100A8/A9 is a potent therapeutic target for idiopathic pulmonary fibrosis. *Journal of molecular medicine (Berlin, Germany)* 99. J Mol Med (Berl): 131–145. https://doi.org/10.1007/S00109-020-02001-X.
87. Anderton, Stephen M., Ruurd van der Zee, and John A. Goodacre. 1993. Inflammation activates self hsp60-specific T cells. *European journal of immunology* 23. Eur J Immunol: 33–38. https://doi.org/10.1002/EJI.1830230107.
88. Moré, S. H., M. Breloer, and A. von Bonin. 2001. Eukaryotic heat shock proteins as molecular links in innate and adaptive immune responses: Hsp60-mediated activation of cytotoxic T cells. *International Immunology* 13. Oxford Academic: 1121–1127. https://doi.org/10.1093/INTIMM/13.9.1121.
89. de Bruyn Carlier, Tina, Fariza Mishaal Saiema Badloe, Johannes Ring, Jan Gutermuth, and Inge Kortekaas Krohn. 2021. Autoreactive T cells and their role in atopic dermatitis. *Journal of Autoimmunity* 120. Academic Press: 102634. https://doi.org/10.1016/J.JAUT.2021.102634.
90. Russotto, Vincenzo, Andrea Cortegiani, Santi Maurizio Raineri, and Antonino Giarratano. 2015. Bacterial contamination of inanimate surfaces and equipment in the intensive care unit. *Journal of Intensive Care*. BioMed Central Ltd. https://doi.org/10.1186/s40560-015-0120-5.
91. Costerton, J. W., Philip S. Stewart, and E. P. Greenberg. 1999. Bacterial biofilms: A common cause of persistent infections. *Science*. https://doi.org/10.1126/science.284.5418.1318.
92. Kyle, Daniel J.T., Antonios Oikonomou, Ernie Hill, and Ardeshir Bayat. 2015. Development and functional evaluation of biomimetic silicone surfaces with hierarchical micro/nano-topographical features demonstrates favourable invitro foreign body response of breast-derived fibroblasts. *Biomaterials* 52. Elsevier Ltd: 88–102. https://doi.org/10.1016/j.biomaterials.2015.02.003.

 doi:10.20944/preprints202212.0004.v1

93. Shin, Byung Ho, Byung Hwi Kim, Sujin Kim, Kangwon Lee, Young Bin Choy, and Chan Yeong Heo. 2018. Silicone breast implant modification review: Overcoming capsular contracture. *Biomaterials Research*. BioMed Central Ltd. https://doi.org/10.1186/s40824-018-0147-5.